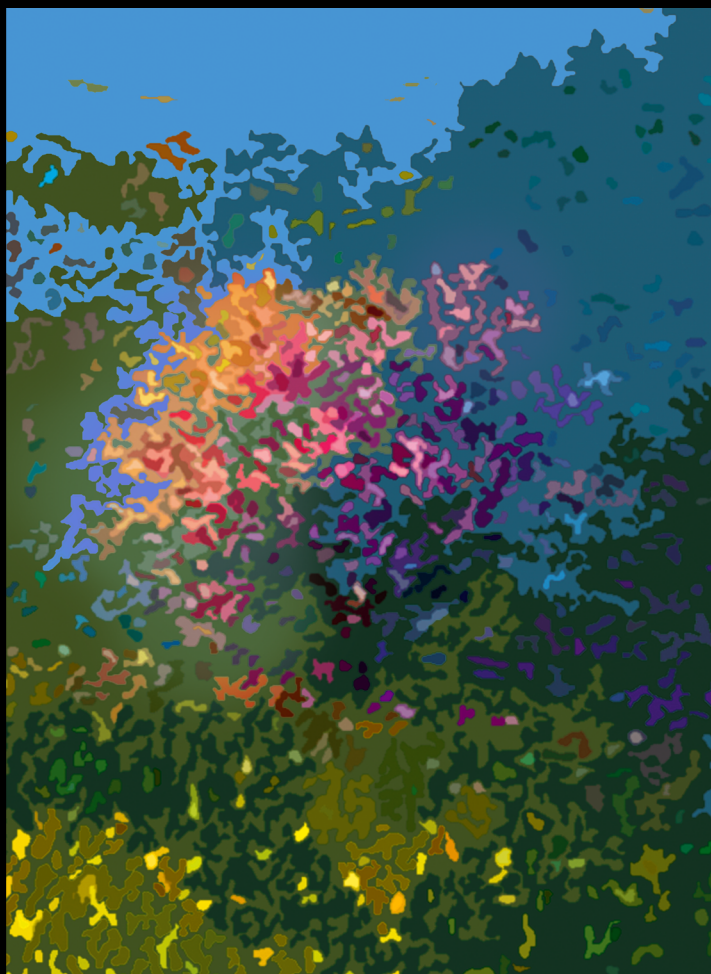




ISTITUTO NAZIONALE DI FISICA NUCLEARE
Laboratori Nazionali di Frascati

FRASCATI PHYSICS SERIES



Fourth Young Researchers Workshop
"Physics Challenges in the LHC Era"

2014

Editor:
Enrico Nardi

FRASCATI PHYSICS SERIES

Series Editor

Rossana Centioni

Technical Editor

Debora Bifaretti

Cover by Claudio Federici

Volume LIX

*Istituto Nazionale di Fisica Nucleare – Laboratori Nazionali di Frascati
Divisione Ricerca
SIDS – Servizio Informazione e Documentazione Scientifica
Ufficio Biblioteca e Pubblicazioni
P.O. Box 13, I-00044 Frascati Roma Italy
email: sis.publications@lnf.infn.it*

Copyright © 2014 by INFN

All rights reserved. No part of this publication may be reproduced, stored in a retrieval system or transmitted in any form or by any means, electronic, mechanical, photocopying, recording or otherwise, without the prior permission of the copyright owner.

ISBN 978-88-86409-66-7

**Fourth Young Researchers Workshop
“Physics Challenges in the LHC Era”
2014**

International Scientific Committee:

Guido Altarelli (*U. & INFN Roma3*)
Wilfried Buchmuller (*DESY*)
Filippo Ceradini (*U. & INFN Roma3*)
Anna Di Ciaccio (*U. & INFN Tor Vergata*)
John Ellis (*CERN*)
Benjamin Grinstein (*UC San Diego*)
Ida Peruzzi (*INFN-LNF & U. Perugia*)
Antonio Pich (*U. Valencia & IFIC, U. Valencia*)
Roberto Fiore (*U. Calabria & INFN Cosenza*)

Local Organizing Committee:

Mario Antonelli
Giuseppe Bevilacqua
Gennaro Corcella
Vittorio Del Duca
Martín González Alonso
Gino Isidori
Maria Paola Lombardo
Andrea Longhin
Aurora Meroni
Enrico Nardi (School Director)
Eduardo Peinado
Tommaso Spadaro

CONTENTS

Preface		VI
Gaetana Anamiati	Z^0 inclusion at leading order in DISENT Monte Carlo	1
Carolina Arbez	LHC-scale left-right symmetry, unification and Dark Matter	8
Simone Biondini	Effective field theory: from Cosmology to Quark Gluon Plasma	14
Sofiane Boucenna	Calculable neutrino masses from gauge lepton number violation	20
Aleksander Gajos	A direct test of T symmetry in the neutral K meson system with $K_S K_L \rightarrow \pi l \nu$ and $K_L \rightarrow 3\pi^0$ at the KLOE-2 experiment	26
Daria Kaminska	Status of measurement of $K_S \rightarrow \pi e \nu$ branching ratio and lepton charge asymmetry with the KLOE detector	32
Martin Krauss	Testing Models with Higher Dimensional Effective Interactions at the LHC and Dark Matter Experiments	38
Riccardo Manzoni	Evidence of the SM Higgs Boson in the Decay Channel into Tau Leptons	44
Nestor Quintero	Di-leptons production in the top quark decay and New Physics	50
Marco Sessa	Construction and performance study of Micromegas muon chambers for ATLAS upgrade	56

PREFACE

The fourth Young Researcher Workshop "Physics Challenges in the LHC Era" was held in the Frascati Laboratories during May 12th and 15th 2014, in conjunction with the XVII edition of the Frascati Spring School "Bruno Touschek".

The Frascati Young Researcher Workshops started with the 2009 Frascati Spring School, and by now represent a well established and important appointment for graduate students in theoretical and experimental high energy and astroparticle physics. Young researchers are invited to present the results of their research work in a fifteen minutes talk, and discuss them with their colleagues. Students have to learn how to condense their results in a short presentation, how to organize a speech on a specialized subject in a way understandable to their colleagues, they get a training in preparing the write up of their contribution for the Workshop Proceedings, they experience how to interact with the Scientific Editor and with the Editorial Office of the Frascati Physics Series and, in many cases, they learn for the first time the procedure to submit their contribution in the arXiv.org database. Helping to develop all these skills is an integral part of the scientific formation the Frascati Spring School is providing.

These proceedings collect the joint efforts of the speakers of the Young Researchers Workshop 2014. The short write-ups represent the best demonstration of the remarkable scientific level of the Workshop contributors, and set the benchmark for the scientific level required to apply for participating in the Workshop.

The success of the XVII Frascati Spring School "Bruno Touschek" and of the joint 4th Young Researcher Workshop "Physics Challenges in the LHC Era" relies on the efforts of a close-knit and well geared team of colleagues. A special acknowledgment goes to Maddalena Legramante, that carried out with her usual efficiency the secretariat work both for the Workshop and for the Spring School, to Claudio Federici, that always puts a special dedication in realizing the beautiful graphics for the Spring School posters and front page of the proceedings, and to Debora Bifaretti for the technical editing. I also want to thank the director of the LNF Research Division Fabio Bossi and the former director Vitaliano Chiarella, the responsabile of the SIDS Rossana Centioni and the former responsabile Danilo Babusci, and the responsabile of the LNF seminars Manuela Boscolo, for sponsoring the XVI Spring School and for their precious help. Finally, a special thanks goes to the Director of the Frascati Laboratories Prof. Umberto Dosselli for his encouragement and unconditional support.

Frascati, September 2014

Enrico Nardi

Inclusion of the Z^0 at the order α_s in the Monte Carlo DISENT

Gaetana Anamiati

Università della Calabria and INFN, Gruppo collegato di Cosenza, Italy

Abstract

Even after the final shutdown of the HERA experiment, the precision in the determination of the strong coupling constant (α_s) and the parton distribution functions can be improved by re-analysing data through Monte Carlo's which include subleading effects. We consider the Monte Carlo program DISENT for jet production at HERA, that in the original version contains only the photon exchange and modify it to include the Z^0 boson exchange at the order α_s . We show some numerical results obtained thereafter.

1 Introduction

Deep inelastic lepton-nucleon scattering (DIS) provides a testing ground for *Quantum Chromodynamics* (QCD) ¹⁾. According to the parton model ^{2, 3)}, the scattering does not occur with the proton as a whole, but with one of its

constituents, called parton, that carries a momentum fraction (x) of the proton momentum with a certain probability density, the so-called parton distribution function $f_i(x)$ (see, *e.g.*, Ref. ⁴), where i is the parton index. Then, the cross section is written as the convolution of these parton distribution functions with the partonic cross section (factorization theorem):

$$d\sigma = \sum_i \int dx f_i(x, \mu_F) d\hat{\sigma}_{ei}(x, \alpha_s(\mu_R^2), \mu_R^2, \mu_F^2). \quad (1)$$

The key point of this theorem is that the parton distribution functions are universal, namely process-independent, and the dependence on the particular process only enters in the partonic cross section, that can be calculated in perturbative QCD as an expansion in α_s ,

$$d\hat{\sigma} = d\hat{\sigma}^{(0)} + \alpha_s d\hat{\sigma}^{(1)} + \alpha_s^2 d\hat{\sigma}^{(2)} + \dots, \quad (2)$$

thanks to the asymptotic freedom property of QCD. The dependence on the renormalization scale μ_R and the factorization scale μ_F arises from the renormalization procedure. When evaluating higher-order QCD cross sections, one has to consider real emission contributions and virtual corrections and one has to deal with different kinds of singularities. In particular, high-momentum regions produce ultraviolet singularities, while soft and collinear regions produce infrared singularities (see, *e.g.*, Ref. ⁵). Both these singularities are regularized by the *dimensional regularization* (see, *e.g.*, Ref. ⁶); to remove the ultraviolet singularities we consider the customary renormalization procedure (see, *e.g.*, Ref. ⁷), while the cancellation of infrared divergences is guaranteed by the *Kinoshita-Lee-Nauenberg* ^{8, 9} theorem, if the final state is inclusive enough. Although the sum of real and virtual contributions is infrared finite, they are separately divergent and therefore unsuitable for the naive inclusion in a Monte Carlo code. Obviously, infrared divergences must be singled out and canceled prior to the numerical calculation; the *Catani-Seymour algorithm* ¹⁰ provides for an efficient, process-independent tool for this purpose.

2 The Monte Carlo program DISENT

The Monte Carlo program DISENT is written in Fortran 77 and runs the calculation of the cross section at α_s^2 for jet production in DIS in the Breit frame.

The main routine is called `disent` and generates the partonic configuration of each event, calculates the contribution to the cross section and returns the results to the `user`. It takes five arguments:

subroutine `disent(NEV, S, NFL, USER, CUTS)`

where

- `NEV` (integer) is the number of events to generate;
- `S` (double precision) is the center of mass energy;
- `NFL` (integer) is the number of flavors.

`User` and `cuts` are two auxiliary subroutines: the first analyses events and selects only those that satisfy certain conditions chosen by the user, according to the selection criteria used in the experimental data; in the second one, the user imposes kinematical limits according to the type of cross section he wants to calculate.

To include the Z^0 boson exchange at α_s order in `DISENT` program, it is necessary to modify only those subroutines related to the calculations of the transition amplitudes. For more details on the structure of these transition amplitudes, see Ref. 11).

At first, we initialize the parameters related to weak interactions, as the Z^0 mass term M_Z^0 , the Weinberg angle $\sin^2 \theta_W$, the third component of the weak isospin and charge of the i -th quark, t_i and e_i , and the couplings $v_i = t_i - 4e_i \sin^2 \theta_W$, $a_i = 2t_i$, $v_i = -1 + 4 \sin^2 \theta_W$, $a_i = -1$; then, we define the following functions:

$$\begin{aligned} A_i(Q^2) &= e_i^2 - 2e_i v_e v_i \chi + (v_e^2 + a_e^2)(v_i^2 + a_i^2) \chi^2, \\ B_i(Q^2) &= -(2e_i a_e a_i \chi - 4v_e a_e v_i a_i \chi^2), \\ \chi(Q^2) &= \frac{1}{(2 \sin 2\theta_W)^2} \frac{Q^2}{Q^2 + M_{Z^0}^2}. \end{aligned}$$

At last, considering only the hard processes contributing at the order α_s , we carry out the following replacements:

- $e^-(l) + q(p_0) \rightarrow e^-(l') + q(p_1)$ (Born),
- $$\sum_{i=q,\bar{q}} e_i^2 f_i(\eta) \overline{|M_{q \rightarrow q}^{(pc)}|^2} \quad (3)$$

$$\longrightarrow \sum_{i=q,\bar{q}} A_i(Q^2) f_i(\eta) \overline{|M_{q \rightarrow q}^{(pc)}|^{-2}} + \sum_{i=q} B_i(Q^2) \Delta f_i(\eta) \overline{|M_{q \rightarrow q}^{(pv)}|^{-2}},$$

where $\Delta f_q(x) \equiv f_q(x) - f_{\bar{q}}(x)$;

- $e^-(l) + q(p_0) \rightarrow e^-(l') + q(p_1) + g(p_2)$ (Born),

$$\sum_{i=q,\bar{q}} e_i^2 f_i(\eta) \overline{|M_{q \rightarrow qg}^{(pc)}|^{-2}} \quad (4)$$

$$\longrightarrow \sum_{i=q,\bar{q}} A_i(Q^2) f_i(\eta) \overline{|M_{q \rightarrow qg}^{(pc)}|^{-2}} + \sum_{i=q} B_i(Q^2) \Delta f_i(\eta) \overline{|M_{q \rightarrow qg}^{(pv)}|^{-2}},$$

- $e^-(l) + g(p_0) \rightarrow e^-(l') + q(p_1) + \bar{q}(p_2)$ (Born),

$$\sum_{i=q,\bar{q}} e_i^2 f_i(\eta) \overline{|M_{g \rightarrow \bar{q}q}^{(pc)}|^{-2}} \quad (5)$$

$$\longrightarrow \sum_{i=q} A_i(Q^2) f_g(\eta) \overline{|M_{g \rightarrow \bar{q}q}^{(pc)}|^{-2}} + \sum_{i=q} B_i(Q^2) f_g(\eta) \overline{|M_{g \rightarrow \bar{q}q}^{(pv)}|^{-2}}.$$

In the expressions above, the apex (pc) stands for “parity conserving” and $M^{(pc)}$ denotes the contributions from the photon exchange only. The effect of the Z^0 exchange amounts to replace e_i^2 with $A_i(Q^2)$ and to introduce a new “parity violating” term, labeled with the apex (pv) and proportional to $B_i(Q^2)$. For the expressions of all amplitudes $M^{(pc,pv)}$ above, we refer to Ref. ¹¹).

We observe that the contribution from

- $e^-(l) + q(p_0) \rightarrow e^-(l') + q(p_1)$ (interference Born and 1-loop)

is factorized as the Born amplitude times a term which contains the divergence, therefore its modification goes together with the first of the replacements listed above.

3 Numerical results and conclusions

We present in the table and in the figure the results of the numerical analysis of 20 million events for the 1-jet inclusive production cross section as a function of Q^2 in the original version in which the program contained only the photon

exchange and in our implementation with the inclusion of the Z^0 exchange. It is possible to notice an increase of the cross section as Q^2 grows, up to about 50% for the largest Q^2 bin.

Q^2 [GeV ²]	$d\sigma/dQ^2$ [pb/GeV ²] (γ)	$d\sigma/dQ^2$ [pb/GeV ²] ($\gamma + Z^0$)
125 – 250	$(8.172 \pm 0.037) \cdot 10^{-1}$	$(8.188 \pm 0.037) \cdot 10^{-1}$
250 – 500	$(2.767 \pm 0.011) \cdot 10^{-1}$	$(2.782 \pm 0.011) \cdot 10^{-1}$
500 – 1000	$(7.450 \pm 0.025) \cdot 10^{-2}$	$(7.563 \pm 0.026) \cdot 10^{-2}$
1000 – 2000	$(1.670 \pm 0.005) \cdot 10^{-2}$	$(1.745 \pm 0.006) \cdot 10^{-2}$
2000 – 5000	$(2.485 \pm 0.007) \cdot 10^{-3}$	$(2.842 \pm 0.008) \cdot 10^{-3}$
5000 – 100000	$(1.800 \pm 0.005) \cdot 10^{-5}$	$(2.656 \pm 0.007) \cdot 10^{-5}$

Table 1: Numerical results for differential cross section as a function of Q^2

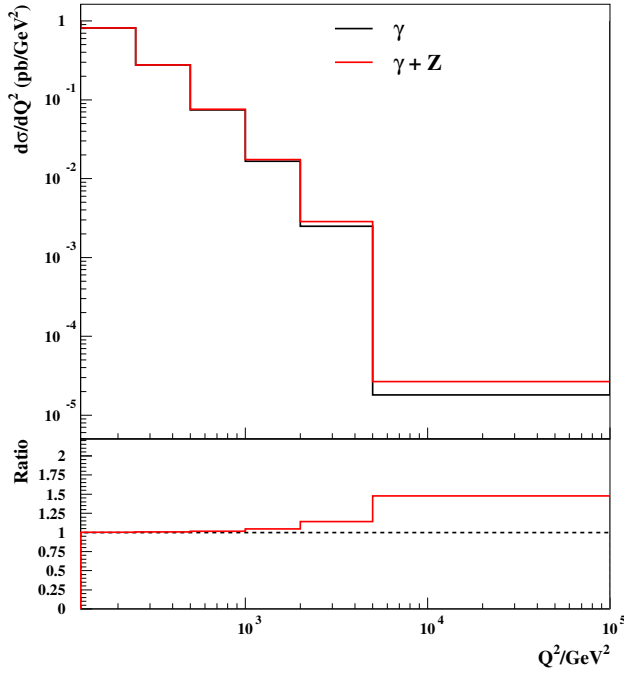


Figure 1: Differential cross section as a function of Q^2

4 Acknowledgements

I would like to express my deep gratitude to Professor Alessandro Papa and Professor Enrico Tassi for their enthusiastic encouragement and their useful critiques during the development of this research work. Their willingness to give me their time so generously has been very much appreciated.

References

1. H. Fritzsch, M. Gell-Mann e H. Leutwyler, *Phys. Lett.* **47B**, 365 (1973).
2. J.D. Bjorken, E.A. Paschos, *Phys. Rev.* **185**, 1975 (1969).
3. R.P. Feynman, *Photon-hadron interactions*, Addison-Wesley (1972).
4. F.E. Close, *An introduction to quarks and partons*, Academic Press (1979).
5. T. Muta, *Foundations of Quantum Chromodynamics*, World Scientific (1987).
6. F. Mandl and G. Shaw. *Quantum Field Theory*, Wiley (1986).
7. M.E. Peskin, D.V. Schroeder, *An introduction to quantum field theory*, Addison-Wesley (1995).
8. T. Kinoshita, *J. Math. Phys.* **3**, 650 (1962); T. Kinoshita, A. Ukawa, *Phys. Rev.* **D13**, 1573 (1976).
9. T.D. Lee, M. Nauenberg, *Phys. Rev.* **B133**, 1549 (1964).
10. S. Catani, M.H. Seymour, *Nucl. Phys.* **B485**, 291-419 (1996).
11. E. Mirkes, *Theory of jets in deep inelastic scattering*, hep-ph/9711224.

LHC-SCALE LEFT-RIGHT SYMMETRY, UNIFICATION AND DARK MATTER

Carolina Arbeláez

Instituto de Física Corpuscular IFIC - Universidad de Valencia

Proceedings based in the paper

Phys.Rev.D89 (2014) 035002

Abstract

In this work we construct a comprehensive list of non-SUSY $SO(10)$ models with left-right symmetric intermediate stage close to the TeV scale which unify better than the MSSM. These models, which contain few extra fields added to the SM, pass some phenomenological constraints like compatibility with the quark and lepton masses and mixings, the current proton decay limits, perturbativity and neutrino masses. We pay special attention to the uncertainties and their role in the determination of the LR-breaking scale. Finally, a connection between DM and nonSUST GUTs is explored.

1 Introduction

Left-right LR models have not been studied very much in the literature in the context of Gauge Coupling Unification (GCU). It is however quite straightforward to construct such a model even with the LR scale close to the EW scale.

Some examples of these models have been proposed, for example, the SUSY LR models described in [1-3]. An interesting feature of these models is that the scale where the symmetry $U(1)_R \times U(1)_{B-L}$ is broken can slide down from (nearly) m_G to any arbitrary value up to m_Z , without destroying GCU (*sliding scale models*). However, supersymmetry is not needed to construct such low-scale LR models. NonSUSY $SO(10)$ models with low intermediate scales have been also proposed in the literature. In ⁴⁾ we dealt with this kind of scenarios. Models which fulfil some special phenomenological requirements are explored. Below some details are described.

In this work we construct simple nonSUSY low LR scale models with a particle content as small as possible. These models follow a minimal set of conceptual and phenomenological requirements: i) There must be at least one field that breaks the intermediate LR symmetry, in this case $\Phi_{1,1,3,-2}$ or $\Phi_{1,1,2,-1}$, ii) The models must contain the necessary ingredients to generate the non trivial CKM matrix. iii) the couplings must be bigger than zero at the GUT scale m_G and iv) the m_G scale should be large enough to prevent fast proton decay.

In these kind of models it is particularly difficult to get a good grip on the GUT scale from a mere renormalization group equations (RGE) running. The uncertainties as well as the threshold effects play a key role in the determination of these scales. Our ignorance of the thresholds should be included as the theoretical error once the two loop coefficients are used in the calculations. It is convenient then to determine m_G and its error by means of a χ^2 optimization based on an educated guess of the relevant theory error. Uncertainties for the prediction of the LR scale and proton decay half-life in the different models will be discussed in more detail in the Section 3.

Dark matter can be also successfully explained in non SUSY $SO(10)$ LR models ^{5, 6)}. Finally we explore the possibility to connect DM with this kind of scenarios, where the symmetry $Z_2 = -1^{3(B-L)}$ which stabilize DM is a remnant symmetry after the breaking $SO(10) \rightarrow SU(3) \times SU(2)_L \times SU(2)_L \times U(1)_{B-L}$.

2 Models

In this section we discuss simple models inspired in $SO(10)$ unification with LR intermediate scale m_{LR} . In the LR stage we consider a total of 24 different representations up to the 126 of $SO(10)$. These representations and the transformation properties of the allowed fields are listed in Table IV of ⁴⁾. As discussed previously, some conditions must be fulfilled in our configurations to have models which are phenomenologically interesting.

Here, two classes of scenarios are analyzed: the scalar and fermion CKM models. In the former, a realistic CKM is generated by the extension of the scalar sector. Here, two bidoublets $\Phi_{1,2,2,0}$ plus an extra scalar $\Phi_{1,1,3,0}$ are added to generate a non-trivial CKM matrix. Considering the 24 fields in Table IV ⁴⁾, a plethora of these kind of models can be constructed. In Table 1 we give few examples.

Configuration	m_{LR} [GeV]	$T_{1/2}$ [y]
$\Phi_{1,2,2,0} + \Phi_{1,1,3,0} + 3\Phi_{1,1,3,-2}$	$1 \cdot 10^2$	$10^{30.6 \pm 2.5}$
$\Phi_{1,2,2,0} + 3\Phi_{1,1,3,0} + 2\Phi_{1,1,3,-2}$	$2 \cdot 10^3$	$10^{31.3 \pm 2.5}$
$2\Phi_{1,2,2,0} + \Phi_{1,1,3,0} + \Phi_{8,1,1,0} + 2\Phi_{1,1,3,-2}$	$5 \cdot 10^2$	$10^{41.3 \pm 2.5}$
$3\Phi_{1,2,2,0} + \Phi_{1,1,3,0} + 3\Phi_{6,1,1,4/3} + 2\Phi_{1,3,1,-2} + \Phi_{3,1,2,-2}$	$4 \cdot 10^2$	$10^{36.3 \pm 2.5}$

Table 1: Simple possible LR models

All the configurations in the Table 1 can explain CKM and conserve parity, except the last one. We can note also that, at the price of introducing one coloured field, the proton decay half life constraint can be completely evaded. It is worthy to mention here that all the models with a second bidoublet $\Phi_{1,2,2,0}$ but no additional coloured particles will have a GUT scale below that $m_G = 2 \times 10^{15}$ GeV, then proton decay half-life values are low. This will be seen in more detail in section 3.

This kind of analysis can be done also for models with additional fermions, like in Table II ⁴⁾, but here we do not enter in detail. Just to mention that a non-trivial CKM can be generated extending the fermion sector by three kind

of fields, corresponding to vector like copies of the SM fields: u^c, d^c and Q .

3 Uncertainties

In this section we discuss uncertainties for the predictions of our LR models. In these scenarios, once the particle content is fixed, essentially three free parameters remain: m_{LR} , m_G and α_G . These parameters can be fixed up to some error by the requirement of gauge coupling unification. In this analysis we used a χ^2 minimization which fit the three measured SM couplings $\alpha_1^{-1}(m_Z)$, $\alpha_2^{-1}(m_Z)$, $\alpha_3^{-1}(m_Z)$ as a function of the three unknown parameters. The error used in the analysis can be divided in an experimental error plus a theory error. In addition, our ignorance of the thresholds should be included as the theoretical error once two-loop coefficients are used in the calculations.

The theory error, which will be always much larger than the experimental error, is calculated using three different assumptions (which are given in detail in ⁴) and also considering that the 1-loop thresholds are formally of the order of 2-loop level effects. Figure 1 shows the allowed parameter space for the configuration $\Phi_{1,2,2,0} + 3\Phi_{1,1,3,0} + 2\Phi_{1,1,3,-2}$ using one of the sets of the theory error $\Delta\alpha_{theory}^{-1}$, Sec 4 ⁴).

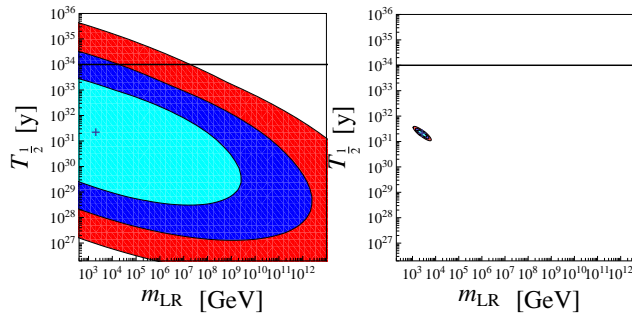


Figure 1: Contour plot of the χ^2 distribution in the plane $(m_{LR}, T_{1/2})$ for the model: SM + $\Phi_{1,2,2,0} + 3\Phi_{1,1,3,0} + 2\Phi_{1,1,3,-2}$. The cyan (blue, red) region corresponds to the allowed region at 68 % (95 % and 3- σ) CL. Left: Using theory error $\Delta\alpha_{theory}^{-1} = 0.7$. Right: χ^2 distribution without theory error.

We can conclude first that the model is excluded by the lower limit of proton decay half-life from Super-K ^{7, 8}) at 1- σ of c.l, but allowed at 2- σ and 3- σ

CL. We can see also that although the preferred value of the m_{LR} scale is within the reach of the LHC, the upper limit on m_{LR} is very large. So m_{LR} is weakly constrained. Therefore the model is not excluded by direct accelerator searches, but may be excluded by a slight improvement in the error calculation and limits on proton decay. Finally, for the right plot it is clear that, without including the theory error in the analysis, the model is completely excluded.

This analysis was also done for a fermion-like CKM configuration. In this case, the proton decay fits better than for the scalar CKM models. This is expected, considering that the GUT scale is quite high in this kind of model due to the coloured fields, as discussed before.

4 Dark Matter and GUTs

In GUTs like $SO(10)$ a discrete $Z_2 = (-1)^{3(B-L)}$ symmetry remains after the $SO(10)$ symmetry breaking $SO(10) \rightarrow SU(3)_c \times SU(2)_L \times SU(2)_R \times U(1)_{B-L}$. This symmetry is known as matter parity.

Multiplets which belongs to the **16** and **144** $SO(10)$ -reps are Z_2 -odd while the ones which belong to the **45**, **54**, **126**, etc. $SO(10)$ -reps are Z_2 -even. Then, scalars which belong to the **16** (such as $\chi^c = \Phi_{1,1,2,-1}$) and fermions in the **45** ($\Phi_{1,1,3,-2}$) or **126** ($\Phi_{1,3,1,-2}$) can be possible DM candidates.

Some of the simple configurations found in the last sections can also potentially explain successfully DM. Some simple examples are: $\Phi_{1,2,2,0} + 2\Phi_{1,1,3,0} + 2\Phi_{1,1,2,-1} + 2\Phi_{1,1,3,-2}$, $2\Psi_{3,2,1,1/3} + \Phi_{8,1,1,0} + 4\Phi_{1,1,3,-2}$ and $\Phi_{1,1,2,0} + \Phi_{1,1,2,-1} + 3\Phi_{1,1,3,-2}$. Note that, for the first configuration, the fields $\Phi_{1,2,2,0}$ and $\Phi_{1,1,3,0}$ realize the scalar CKM, $\Phi_{1,1,3,-2}$ breaks the LR symmetry and $\Phi_{1,1,2,-1}$ is the DM candidate.

5 Conclusions

In this work we found a large number of simple nonSUSY models with LR intermediate scales which lead to a remarkably well $SO(10)$ -like gauge coupling unification. A large number of settings pass all the phenomenological con-

straints regarding to compatibility with the CKM mass matrix, current proton decay life times, perturbativity and GCU. In the second part we found that theoretical uncertainties affects the possible determination of the LR scale. The viability of a GUT model depends strongly of the GUT-scale thresholds (two loop effects) and other high-scale effects. Finally we discuss the connection between DM and GUTs. There are a large number of possible configurations to explain DM in a nonSUSY GUT scenario where a Z_2 symmetry remains after the $SO(10)$ symmetry breaking.

6 Acknowledgements

This work is supported in part by EU Network grant UNILHC PITN-GA-2009-237920, Spanish MICINN grants FPA2011-22975, MULTIDARK CSD2009-00064 and the Generalitat Valenciana grant Prometeo/2009/091. C.A also acknowledges help from M. Hirsch, J.C Romão and M. Malinsky.

References

1. M. Malinsky, J. C. Romao, and J. W. F. Valle, Phys.Rev.Lett. **95**, 161801 (2005), arXiv:hep-ph/0506296.
2. V. De Romeri, M. Hirsch, and M. Malinsky, Phys.Rev. **D84**, 053012 (2011), arXiv:1107.3412.
3. C. Arbelaez, R. M. Fonseca, M. Hirsch, and J. C. Romao, Phys.Rev. **D87**, 075010 (2013), arXiv:1301.6085.
4. C. Arbelaez, M. Hirsch, M. Malinsky and J. C. Romo, Phys. Rev. D **89**, 035002 (2014) [arXiv:1311.3228 [hep-ph]].
5. M. Kadastik, K. Kannike and M. Raidal, Phys. Rev. D **80**, 085020 (2009) [Erratum-ibid. D **81**, 029903 (2010)] [arXiv:0907.1894 [hep-ph]].
6. M. Frigerio and T. Hambye, Phys. Rev. D **81**, 075002 (2010) [arXiv:0912.1545 [hep-ph]].
7. Super-Kamiokande Collaboration, K. Abe *et al.*, (2013), arXiv:1305.4391.
8. Super-Kamiokande, H. Nishino *et al.*, Phys.Rev. **D85**, 112001 (2012), arXiv:1203.4030.

Frascati Physics Series Vol. LIX (2014), pp. 00-00
4th YOUNG RESEARCHERS WORKSHOP: “Physics Challenges in the LHC Era”
Frascati, May 12 and 15, 2014

Effective field theories: from Cosmology to Quark Gluon Plasma

Simone Biondini
*Technische Universität München,
Physik Department I, Garching 85747, Germany*

Abstract

Cosmology and particle physics come across a tight connection in the attempt to reproduce and understand quantitatively the results of experimental findings. Indeed, the quark gluon plasma (QGP) found at colliders and the baryon asymmetry abundance provided by the WMAP collaboration are examples where to apply field theoretical techniques in issues relevant for Cosmology.

In the simplest leptogenesis framework, heavy Majorana neutrinos are at the origin of the baryon asymmetry. The non-relativistic regime appears to be relevant during the lepton asymmetry generation where the interactions among particles occur in a thermal medium.

We discuss the development of an effective field theory (EFT) for non-relativistic Majorana particles to simplify calculations at finite temperature. We show an application of such a method to the case of a heavy Majorana neutrino decaying in a hot and dense plasma of Standard Model (SM) particles.

These techniques are analogous to those widely used for the investigation of heavy-ion collisions at colliders by exploiting hard probes. We sketch some commonalities between Majorana neutrinos and quarkonium in medium.

1 Introduction

The physics of the early universe represents a challenge both theoretically and experimentally. Indeed, during the first stages of the universe evolution, particles interact at very high energies, density and temperatures. At present, such extreme conditions might be reproduced only in dedicated facilities.

We observed recently hints at the ALICE experiment ¹⁾, and previously at RICH ²⁾, that the quark gluon plasma is possibly formed. This is a phase in which quarks and gluons are no longer confined in hadrons and this transition is expected to be occurred during the universe evolution. Confirming the existence of this phase of matter and understanding its properties might shed light on our comprehension about particles interactions in the early universe. Quarkonia suppression in medium has been considered a promising probe to study QGP in heavy-ion collisions ³⁾.

Other important processes taking place in the hot and dense universe are the dark matter and baryon asymmetry generation. The WMAP collaboration provides accurate values for the dark matter abundance and the amount of baryon asymmetry ⁴⁾. At variance with the quark gluon plasma, some physics beyond the SM is needed to explain such evidences. Let us focus on the generation of the baryon asymmetry and on a possible attractive solution, embedded in the class of models called leptogenesis.

In its simplest scenario, a net lepton asymmetry is produced in the CP violating decays of heavy Majorana neutrinos into SM leptons and anti-leptons in different amounts ⁵⁾. The lepton asymmetry is then partially reprocessed in a baryon asymmetry via the sphalerons transitions. The interactions of heavy neutrinos with particles in the plasma occur in a hot medium and one has to take into account a field theoretical approach that includes thermal effects.

Either in the case of heavy quarkonium in a quark gluon plasma or heavy Majorana neutrinos in the early universe, the presence of a thermal medium may induce some effects. Much progress has been done in this direction and we discuss here the EFT approach to address the issue.

In section 2, we introduce the EFT formalism we are going to use for a non-relativistic particle. We show how to reproduce the neutrino thermal width by using the EFT techniques in section 3, whereas we sketch the case of

heavy quarkonium in a weakly interacting QGP in section 4.

2 Effective Lagrangian for non-relativistic particles

We define a particle to be heavy when its mass, M , is bigger than any other scale of the medium. For a system in equilibrium the main thermodynamical scale is the temperature, T . The situation we want to consider is $M \gg T$ and in such a case the heavy particle is also non-relativistic. Hence, we can devise an EFT Lagrangian that properly describes the low-energy modes of the heavy particle as the relevant degrees of freedom, labelled with the field N in the following. The effective Lagrangian has the general form

$$\mathcal{L}_{\text{EFT}} = N^\dagger iD_0 N + \sum_n c_n \left(\frac{\mu}{M} \right) \frac{\mathcal{O}_n(\mu, T)}{M^{d_n-4}} + \mathcal{L}_{\text{light}}. \quad (1)$$

The heavy particle is considered in a reference frame at rest up to momentum fluctuations much smaller than M . The heavy particle sector is organized as an expansion in $1/M$. The effective operators, describing the interaction among the heavy and light degrees of freedom, are suppressed with the proper power of M in order to keep the Lagrangian density of dimension four. The higher the operator dimension the bigger the suppression. The light degrees of freedom are embedded in $\mathcal{L}_{\text{light}}$.

The Wilson coefficients, c_n , are the parameters of the low-energy theory and one has to compute them by the matching procedure. Since they encode the effects of the high energy scale, M , one may ignore and set to zero any other scale in the matching calculation, namely $T = 0$. This turns out to be a helpful simplification in the case of calculations in a thermal bath. Indeed, the Wilson coefficients are obtained by matching in-vacuum matrix elements. The temperature only affects the calculation of observables in the low-energy Lagrangian, as we are going to show in the case of the neutrino thermal width in the next section.

3 Thermal width for heavy Majorana neutrinos

We are interested in the thermal width for a Majorana neutrino induced by a thermal bath. We start with the fundamental Lagrangian that includes one additional neutrino to the SM content. The additional lepton is also called

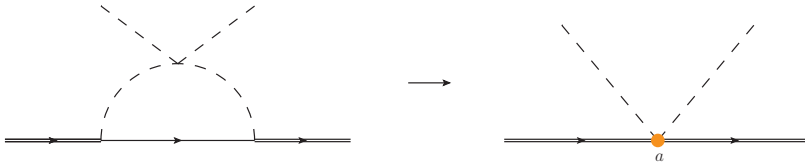


Figure 1: Relevant diagram for the matching computation.

sterile or right-handed neutrino, it has a Majorana mass and interacts only via Yukawa couplings with SM Higgs and leptons. The Lagrangian reads

$$\mathcal{L} = \mathcal{L}_{\text{SM}} + \frac{1}{2}\bar{\psi}i\cancel{\partial}\psi - \frac{M}{2}\bar{\psi}\psi - F_f\bar{L}_f\tilde{\phi}P_R\psi - F_f^*\bar{\psi}P_L\tilde{\phi}^\dagger L_f, \quad (2)$$

where \mathcal{L}_{SM} is the SM Lagrangian, ψ is the Majorana neutrino field, F_f is the Yukawa coupling, L_f stands for the SM lepton doublet with flavour f , $\tilde{\phi} = i\sigma_2\phi^*$ where ϕ is the Higgs field and $P_{L(R)}$ is the left (right) chiral projector. This Lagrangian is not enough to have leptogenesis because there is only one sterile neutrino. However, we take the Lagrangian in (2) as a toy model to implement the EFT treatment for the thermal width. We consider the following hierarchy of scales $M \gg T \gg M_W$, where M_W sets the electroweak scale.

The first step consists in integrating out the energy modes of order M so that we are left with non-relativistic excitations of Majorana neutrinos. The low-energy Lagrangian reads, according to the prototype in eq. (1), as follows

$$\mathcal{L}_{\text{EFT}} = \mathcal{L}_{\text{SM}} + N^\dagger \left(i\partial_0 - i\frac{\Gamma_0}{2} \right) N + \frac{\mathcal{L}^{(1)}}{M} + \frac{\mathcal{L}^{(2)}}{M^2} + \frac{\mathcal{L}^{(3)}}{M^3} + \mathcal{O}\left(\frac{1}{M^4}\right), \quad (3)$$

where Γ_0 is the decay width at $T = 0$. $\mathcal{L}^{(1)}$, $\mathcal{L}^{(2)}$ and $\mathcal{L}^{(3)}$ contain respectively dimension five, six and seven operators. We focus on the only dimension five operator in $\mathcal{L}^{(1)}$, $(a/M)N^\dagger N\phi^\dagger\phi$, to show our procedure. This operator describes the effective interaction between a non-relativistic Majorana neutrino and a SM Higgs boson. By integrating out the energy modes of order M , the one loop process in the fundamental theory is matched onto a four-particle interaction, as shown in Figure 1. Standard $T = 0$ perturbation techniques are exploited. The matching coefficient reads $\text{Im}(a) = -(3\lambda|F_f|^2)/(8\pi)$ and determines the low-energy neutrino-Higgs interaction. We extracted only the imaginary part since it is the one relevant for the determination of the thermal width.

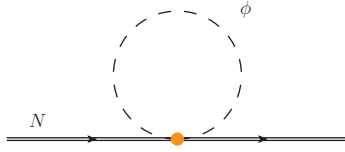


Figure 2: The tadpole diagram in the low-energy theory is shown.

Once the effective Lagrangian is determined, one can calculate the thermal corrections to the width. This is carried out in the low-energy theory, where the dynamical energy modes are those of order T . In the present formalism, the thermal width is obtained by computing the tadpole diagram in Figure 2. A Higgs boson from the thermal bath runs in the loop diagram and the leading thermal correction reads ^{6), 7)}

$$\Gamma_a = 2 \frac{\text{Im}(a)}{M} \langle \phi^\dagger(0) \phi(0) \rangle = -\lambda \frac{|F_f|^2 M}{8\pi} \left(\frac{T}{M} \right)^2. \quad (4)$$

We notice that the derivation of the thermal width is divided into two steps: a one loop calculation in vacuum (matching), and a one loop computation in the EFT (thermal tadpole). In a full relativistic thermal field theory derivation for the thermal width such a simplification can barely arise, whereas it is typical of the EFT approach.

4 Quarkonium suppression in QGP and conclusions

As we mentioned in the introduction, quarkonia suppression in medium may be useful to probe the QGP features. The main difference with respect to Majorana neutrinos is that heavy quarkonium is a bound state of heavy quarks ($Q\bar{Q}$).

This complicates much more the treatment in a thermal medium because of the interplay between non-relativistic and thermodynamic scales. The former are m , mv , and mv^2 , respectively the mass of the heavy quark, the inverse size of the bound state and the binding energy. The temperature, T , and the Debye mass, $m_D = gT$, are the thermodynamic ones. An EFT treatment for a wide range of scales configurations has been established in ⁸⁾. The main outcome is a rigorous derivation of the static potential that comprises a real

and imaginary part with thermal corrections. In particular, the imaginary part of the potential is related with the thermal width of the quarkonium that can be traced back to the interactions between the bound state and the partons in the QCD medium. This is in complete analogy with the Majorana neutrino thermal width that arises from the interactions with the SM particles in the thermal bath. Therefore, the developments of resummation techniques in hot QCD and Cosmology may benefit both fields.

5 Acknowledgments

I would like to thank N. Brambilla, M. Escobedo and A. Vairo for the collaboration on the work presented here based on ⁹⁾, and the organizers of the *4th Young Researchers Workshop* for the possibility to give a talk.

References

1. K. Aamodt *et al.* [ALICE Collaboration], Phys. Lett. B **696** (2011) 30 [arXiv:1012.1004 [nucl-ex]].
2. STAR collaboration, Phys. Lett. B **567** (2003) 167.
3. T. Matsui and H. Satz, Phys. Lett. B **178** (1986) 416.
4. G. Hinshaw *et al.* [WMAP Collaboration], Astrophys. J. Suppl. **208** (2013) 19 [arXiv:1212.5226 [astro-ph.CO]].
5. M. Fukugita and T. Yanagida, Phys. Lett. B **174** (1986) 45.
6. A. Salvio, P. Lodone and A. Strumia, JHEP **1108** (2011) 116 [arXiv:1106.2814 [hep-ph]].
7. M. Laine and Y. Schroder, JHEP **1202** (2012) 068 [arXiv:1112.1205 [hep-ph]].
8. N. Brambilla, J. Ghiglieri, A. Vairo and P. Petreczky, Phys. Rev. D **78** (2008) 014017 [arXiv:0804.0993 [hep-ph]].
9. S. Biondini, N. Brambilla, M. A. Escobedo and A. Vairo, JHEP **1312** (2013) 028 [arXiv:1307.7680, arXiv:1307.7680].

Frascati Physics Series Vol. XXXX (yyyy)
TITLE
Date

RADIATIVE NEUTRINO MASS FROM GAUGE LEPTON NUMBER VIOLATION

Sofiane M. Boucenna
Instituto de Física Corpuscular (CSIC-Universitat de València)
Apto. 22085, E-46071 Valencia, Spain.

Abstract

We propose a new radiative mechanism for neutrino mass generation based on the $SU(3)_c \otimes SU(3)_L \otimes U(1)_X$ electroweak gauge group. Lepton number is spontaneously broken in the gauge sector only. As a result light Majorana masses arise from neutral gauge boson exchange at the one-loop level. In addition to the isosinglet neutrinos which may be produced at the LHC through the extended gauge boson *portals*, the model contains new quarks which can also lie at the TeV scale and provide a plethora of accessible collider phenomena.

1 Introduction

The origin of neutrino mass and mixing, required in order to account for neutrino oscillation data ^{1, 2)}, poses one of the biggest challenges in particle

physics. While charged fermions must be Dirac particles, neutrinos are generally expected to be Majorana fermions ³⁾, breaking lepton number and inducing neutrinoless double beta decay ⁴⁾.

Another important challenge is the origin of the number of families. We know that three different flavors exist, i.e. states with the same gauge quantum numbers but different mass. But we do not know why nature replicates, nor why the masses of the three generations of Standard Model quarks and leptons are so different, nor why they mix in the way they do (flavor problem).

In ⁵⁾ we considered an alternative approach to neutrino mass generation at accessible scales and "explaining" the number of families. The model is based on the $SU(3)_c \otimes SU(3)_L \otimes U(1)_X$ (3-3-1) electroweak gauge structure and is consistent only if the number of families equals the number of quark colors ^{6, 7)}, giving a reason for having three species of fermions. This feature follows from gauge anomaly cancellation and characterizes 331 models, including other variants e.g. ^{8, 9, 10, 11, 12, 13)}.

2 The model

We start from the $SU(3)_c \otimes SU(3)_L \otimes U(1)_X$ gauge framework suggested in ^{6, 7)}. We concentrate on the electroweak part of the model. The left-handed leptons are assigned to the anti-triplet representation of $SU(3)_L$

$$\psi_L^\ell = \begin{pmatrix} \ell^- \\ \nu_\ell \\ N_\ell^c \end{pmatrix}_L, \quad (1)$$

where $\ell = 1, 2, 3 \equiv e, \mu, \tau$. In addition to the new two-component neutral fermions present in the lepton triplet $N_L^c \equiv (N^c)_L \equiv (\nu_R)^c$ where $\psi^c = C\bar{\psi}^T$ and C is the charge conjugation matrix, we introduce new sequential lepton-number-carrying gauge singlets $S = \{S_1, S_2, S_3\}$ sequentially ^{14, 15, 16, 17, 18)}. The matter content of the model is summarized in Tab. 1.

With the above \mathcal{L} assignment the electric charge and lepton number are given in terms of the $U(1)_X$ generator X and the diagonal generators of the $SU(3)_L$ as $Q = T_3 + \frac{1}{\sqrt{3}}T_8 + X$ and $L = \frac{4}{\sqrt{3}}T_8 + \mathcal{L}$

In order to spontaneously break the weak gauge symmetry, we introduce three scalar anti-triplets $\phi_1 \sim (\mathbf{3}^*, +2/3)$ and $\phi_{2,3} \sim (\mathbf{3}^*, -1/3)$. Note that the third component of ϕ_3 carries two units of lepton number. Following the

	ψ_L^ℓ	ℓ_R	$Q_L^{1,2}$	Q_L^3	\hat{u}_R	\hat{d}_R	S	ϕ_1	ϕ_2	ϕ_3
$SU(3)_c$	1	1	3	3	3	3	1	1	1	1
$SU(3)_L$	3S	1	3	3S	1	1	1	3S	3S	3S
$U(1)_X$	$-\frac{1}{3}$	-1	0	$+\frac{1}{3}$	$+\frac{2}{3}$	$-\frac{1}{3}$	0	$+\frac{2}{3}$	$-\frac{1}{3}$	$-\frac{1}{3}$
\mathcal{L}	$-\frac{1}{3}$	-1	$-\frac{2}{3}$	$+\frac{2}{3}$	0	0	1	$+\frac{2}{3}$	$-\frac{4}{3}$	$+\frac{2}{3}$

Table 1: Matter content of the model, where $\hat{u}_R \equiv (u_R, c_R, t_R, t'_R)$ and $\hat{d}_R \equiv (d_R, s_R, b_R, d'_R, s'_R)$ (see text).

notation of ⁷⁾ we have the following vacuum expectation values (VEVs)

$$\langle \phi_1 \rangle = \begin{bmatrix} k_1 \\ 0 \\ 0 \end{bmatrix}, \langle \phi_2 \rangle = \begin{bmatrix} 0 \\ 0 \\ n_1 \end{bmatrix}, \langle \phi_3 \rangle = \begin{bmatrix} 0 \\ k_2 \\ n_2 \end{bmatrix}, \quad (2)$$

where the k_1 and k_2 VEVs are at the electroweak scale and correspond to the VEV of the $SU(2)_L \subset SU(3)_L$ doublets. The VEVs n_1 and n_2 are isosinglet VEVs that characterize the $SU(3)_L$ breaking scale. Note that while ϕ_3 takes VEV in both electrically neutral directions, the second VEV of ϕ_2 is neglected, so that lepton number is broken only by $SU(2)_L$ singlets. This pattern gives the simplest consistent neutrino mass spectrum, avoiding the linear seesaw contribution ^{19, 20)}.

There are in total nine electroweak gauge bosons, four of which are charged, while five are electrically neutral, namely W^3, W^6, W^8, B and one neutral boson, unmixed if CP is conserved W^7 .

3 Neutrino masses

Turning to the lepton sector, the Yukawa terms are

$$\mathcal{L}_{\text{leptons}} = y_{ij}^\ell \overline{\psi_L^i} l_R^j \phi_1 + y_{ij}^a \psi_L^{iT} C^{-1} \psi_L^j \phi_1 + y_{ij}^s \overline{\psi_L^i} S^j \phi_2 + \text{h.c.}$$

where contraction of the flavor indices $i, j = 1, 2, 3$ is assumed. Here y^ℓ and y^s are arbitrary matrices while y^a is antisymmetric. The charged lepton mass matrix is just $M_\ell = y^\ell \langle \phi_1^0 \rangle$ and can be made diagonal in the usual way. Note that, thanks to an auxiliary parity symmetry, ϕ_3 does not couple to leptons.

The tree level neutrino mass matrix in the basis (ν_L, N^c, S) is given by

$$M_\nu = \begin{pmatrix} 0 & m_D & 0 \\ & 0 & M \\ & & 0 \end{pmatrix}, \quad (3)$$

where $m_D = k_1 y^a$, and $M = n_1 y^s$. Note that lepton number conservation forbids the Majorana mass entry for S . We denote the corresponding eigenstates as ν_1, ν_2, ν_3 . The heavy states form Dirac pairs with masses M_{D_i} ($i = 1, 2, 3$). On the other hand the state ν_1 is massless because of lepton number conservation in Eq. (3). This holds at tree level. However lepton number is broken spontaneously by $n_2 \neq 0$ and as a result induces light neutrino masses radiatively, as illustrated by the diagram in Fig. 1 (left). Indeed, the interplay of the intra-multiplet gauge boson exchange connecting ν to N^c with the gauge boson mixing implies that lepton number is necessarily violated in the neutral fermion sector. As a result the massless neutrino is not protected and radiative corrections involving the gauge bosons will yield a *calculable* Majorana mass term as depicted in the diagram of Fig. 1 and given by

$$m_{\nu_{\text{light}}} \simeq \frac{g^2 \epsilon \beta}{16\pi^2} M_D \frac{m_{Z'}^2}{M_D^2 + m_{Z'}^2} \log \frac{m_{Z'}^2}{M_D^2}, \quad (4)$$

where g is a simple function of gauge coupling constants g_1 and g_2 and ϵ is the mixing of W^6 with W^3, W^8 and B . Note that the contribution proportional to ϵ^2 and β^2 vanish as expected.

Fig. 1 (right) shows the correlation between the light neutrino mass scale and the Z' mass for various values of the Dirac mass M_D , parametrized by the Yukawa coupling y^a . For definiteness we fix the n_2 VEV, responsible for the masses of the new iso-singlet colored states at 1 TeV and 10 TeV. Increasing n_2 would push up the Z' mass and, assuming Yukawas of order one, would increase the exotic quark masses.

4 Conclusion

In summary, we have proposed a new mechanism to generate neutrino mass based on the $SU(3)_L \otimes U(1)_X$ gauge symmetry. At tree level neutrinos are massless because of lepton number conservation. Gauge interactions violate lepton number and lead to a Majorana mass term for light neutrinos at one-loop level. In contrast to most neutrino mass generation schemes, such as the

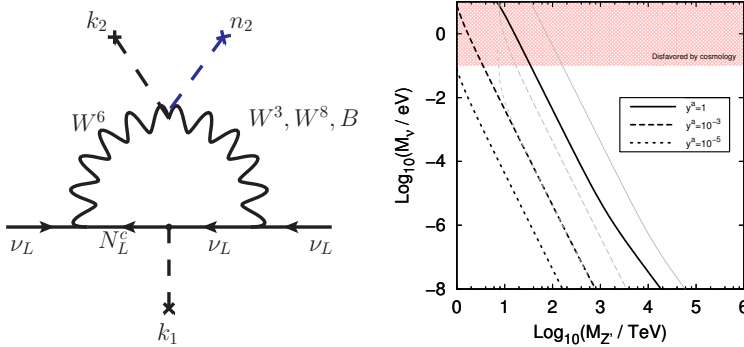


Figure 1: LEFT: Gauge boson exchange diagram for radiatively induced Majorana neutrino mass in the flavor basis. RIGHT: Neutrino mass versus Z' scale for various values of the Dirac mass parameter M_D . Solid, dashed and dot-dashed lines correspond to $y^a = 1, 10^{-3}$ and 10^{-5} respectively. $g_1 = 0.6$ and $k_2 = 90$ GeV and the scale of the new colored states (n_2) is fixed at 1 TeV (thick lines) and 10 TeV (thin lines).

seesaw mechanism, where the neutrino mass comes from Yukawa couplings, here it arises directly from gauge boson exchange as seen in Fig. 1 (left) and Eq. (4). All neutrino species are massive, and their splittings and mixing parameters can be fitted to the oscillation data. Moreover, if light enough, the new exotic colored states would also be produced at the LHC and induce gauge-mediated flavor-changing neutral currents, e.g. $b \rightarrow s\mu^+\mu^-$ (22) providing a double test.

References

1. J. Beringer et al. (Particle Data Group), Phys.Rev. **D86**, 010001 (2012).
2. D. Forero, M. Tortola, and J. W. F. Valle, Phys.Rev. **D86**, 073012 (2012), arXiv:1205.4018.
3. J. Schechter and J. W. F. Valle, Phys. Rev. **D22**, 2227 (1980).
4. J. Schechter and J. W. F. Valle, Phys. Rev. **D25**, 2951 (1982a).
5. S. M. Boucenna, S. Morisi, and J. W. F. Valle, To appear in Phys. Rev. D, arXiv:1405.2332.

6. M. Singer, J. Valle, and J. Schechter, Phys.Rev. **D22**, 738 (1980).
7. J. W. F. Valle and M. Singer, Phys. Rev. **D28**, 540 (1983).
8. R. Foot, H. N. Long, and T. A. Tran, Phys.Rev. **D50**, 34 (1994)
9. P. H. Frampton, Phys. Rev. Lett. **69**, 2889 (1992).
10. F. Pisano and V. Pleitez, Phys.Rev. **D46**, 410 (1992)
11. H. N. Long, Phys.Rev. **D53**, 437 (1996)
12. M. Tully and G. C. Joshi, Phys.Rev. **D64**, 011301 (2001)
13. P. V. Dong, H. T. Hung and T. D. Tham, Phys. Rev. D **87**, 115003 (2013).
14. R. N. Mohapatra and J. W. F. Valle, Phys. Rev. **D34**, 1642 (1986).
15. J. Bernabeu et al., Phys. Lett. **B187**, 303 (1987).
16. M. Dittmar, A. Santamaria, M. C. Gonzalez-Garcia, and J. W. F. Valle, Nucl. Phys. **B332**, 1 (1990).
17. G. C. Branco, M. N. Rebelo, and J. W. F. Valle, Phys. Lett. **B225**, 385 (1989).
18. N. Rius and J. W. F. Valle, Phys. Lett. **B246**, 249 (1990).
19. E. Akhmedov et al., Phys. Lett. **B368**, 270 (1996a) and Phys. Rev. **D53**, 2752 (1996b)
20. M. Malinsky, J. C. Romao, and J. W. F. Valle, Phys. Rev. Lett. **95**, 161801 (2005).
21. H. Georgi and S. L. Glashow, Phys.Rev. **D6**, 429 (1972).
22. A. J. Buras, F. De Fazio and J. Girrbach, JHEP **1402**, 112 (2014) [arXiv:1311.6729 [hep-ph], arXiv:1311.6729].

**A direct test of \mathcal{T} symmetry in the neutral K meson system with
 $K_S \rightarrow \pi \ell \nu$ and $K_L \rightarrow 3\pi^0$ at KLOE-2**

Aleksander Gajos
on behalf of the KLOE-2 Collaboration
Institute of Physics, Jagiellonian University, Cracow, Poland

Abstract

Quantum entanglement of K and B mesons allows for a direct experimental test of time-reversal symmetry independent of \mathcal{CP} violation. The \mathcal{T} symmetry can be probed by exchange of initial and final states in the reversible transitions between flavor and CP-definite states of the mesons which are only connected by the \mathcal{T} conjugation. While such a test was successfully performed by the BaBar experiment with neutral B mesons, the KLOE-2 detector can probe \mathcal{T} -violation in the neutral kaons system by investigating the process with $K_S \rightarrow \pi^\pm l^\mp \nu_l$ and $K_L \rightarrow 3\pi^0$ decays. Analysis of the latter is facilitated by a novel reconstruction method for the vertex of $K_L \rightarrow 3\pi^0$ decay which only involves neutral particles. Details of this new vertex reconstruction technique are presented as well as prospects for conducting the direct \mathcal{T} symmetry test at the KLOE-2 experiment.

1 Introduction

A direct test of the time-reversal symmetry in a single experiment is of great interest among possible ways to probe the \mathcal{T} symmetry violation ¹⁾. For particles with spin 0 such as pseudo-scalar mesons, a direct test may be obtained by observation of an asymmetry between a reaction from state i to state f and a reversed reaction $f \rightarrow i$. While the CPLEAR experiment measured a nonzero value of the Kabir asymmetry in neutral kaon oscillations ²⁾, a controversy was raised as to whether this result was independent of \mathcal{CP} violation as the $K^0 \rightarrow \bar{K}^0$ and $\bar{K}^0 \rightarrow K^0$ transitions are connected by both the \mathcal{T} and \mathcal{CP} symmetries. Therefore, an idea was proposed to exploit the quantum correlations of neutral B and K meson pairs to observe reversible transitions between flavour and \mathcal{CP} -definite states of the mesons ^{3, 4)}. Such a \mathcal{T} symmetry test was successfully performed by the BaBar experiment with the entangled neutral B meson system ⁵⁾. In turn, the KLOE-2 detector at the DAΦNE ϕ -factory is capable of performing a statistically significant direct observation of \mathcal{T} symmetry violation with neutral kaons independently of \mathcal{CP} violation ⁴⁾.

2 Transitions between flavour and \mathcal{CP} -definite neutral kaon states

Neutral kaon states may be described in a number of bases including flavour-definite states:

$$\mathcal{S} |K^0\rangle = +1 |K^0\rangle, \quad \mathcal{S} |\bar{K}^0\rangle = -1 |\bar{K}^0\rangle, \quad (1)$$

as well as the states with definite \mathcal{CP} parity:

$$|K_+\rangle = \frac{1}{\sqrt{2}} [|K^0\rangle + |\bar{K}^0\rangle] \quad \mathcal{CP} = +1, \quad (2)$$

$$|K_-\rangle = \frac{1}{\sqrt{2}} [|K^0\rangle - |\bar{K}^0\rangle] \quad \mathcal{CP} = -1. \quad (3)$$

State of the kaon can be identified at the moment of decay through observation of the decay final state. With the assumption of $\Delta S = \Delta Q$ rule¹, semileptonic kaon decays with positively and negatively charged leptons (later denoted as ℓ^+ , ℓ^-) unambiguously identify the decaying state as K^0 and \bar{K}^0 respectively. Similarly, the \mathcal{CP} -definite states K_+ and K_- are implied by decays to hadronic

¹Althought an assumption, the $\Delta S = \Delta Q$ rule is well tested in semileptonic kaon decays ⁶⁾

final states with respectively two and three pions (denoted $\pi\pi$, 3π). In order to observe a transition between the $\{K^0, \bar{K}^0\}$ and $\{K_+, K_-\}$ states, both the *in* and *out* states must be identified in the respective basis. This is uniquely possible in the entangled system of neutral K mesons produced at a ϕ -factory. Due to conservation of $\phi(1^{--})$ quantum numbers, the $\phi \rightarrow K^0 \bar{K}^0$ decay yields an anti-symmetric non-strange final state of the form:

$$|\phi\rangle \rightarrow \frac{1}{\sqrt{2}} (|K^0(+\vec{p})\rangle |\bar{K}^0(-\vec{p})\rangle - |\bar{K}^0(+\vec{p})\rangle |K^0(-\vec{p})\rangle), \quad (4)$$

which exhibits quantum entanglement between the two kaons in the EPR sense ⁷⁾. Thus, at the moment of decay of first of the K mesons (and, consequently, identification of its state) state of the partner kaon is immediately known to be orthogonal. This property allows for identification of state of the still-living kaon only by observing the decay of its partner. Its state can be then measured at the moment of decay after time Δt , possibly leading to observation of a transition between strangeness and CP-definite states. A list of all possible transitions is presented in Table 1. It is immediately visible that time-reversal conjugates of these transitions are not identical with neither their CP- nor CPT-conjugates which is crucial for independence of the test.

	Transition	\mathcal{T} -conjugate
1	$K^0 \rightarrow K_+ \quad (\ell^-, \pi\pi)$	$K_+ \rightarrow K^0 \quad (3\pi^0, \ell^+)$
2	$K^0 \rightarrow K_- \quad (\ell^-, 3\pi^0)$	$K_- \rightarrow K^0 \quad (\pi\pi, \ell^+)$
3	$\bar{K}^0 \rightarrow K_+ \quad (\ell^+, \pi\pi)$	$K_+ \rightarrow \bar{K}^0 \quad (3\pi^0, \ell^-)$
4	$\bar{K}^0 \rightarrow K_- \quad (\ell^+, 3\pi^0)$	$K_- \rightarrow \bar{K}^0 \quad (\pi\pi, \ell^-)$

Table 1: Possible transitions between flavour and CP-definite states and their time-reversal conjugates. For each transition a time-ordered pair of decay products which identifies the respective states is given.

3 Observables of the test

For each of the transitions from Table 1 occurring in time Δt and its time-reversal conjugate a time-dependent ratio of probabilities can be defined as an observable of the \mathcal{T} symmetry test. In the region where high statistics is

expected at KLOE-2, however, two of them are important for the test:

$$R_2(\Delta t) = \frac{P[\text{K}^0(0) \rightarrow \text{K}_-(\Delta t)]}{P[\text{K}_-(0) \rightarrow \text{K}^0(\Delta t)]} \sim \frac{\text{I}(\ell^-, 3\pi^0; \Delta t)}{\text{I}(\pi\pi, \ell^+; \Delta t)}, \quad (5)$$

$$R_4(\Delta t) = \frac{P[\bar{\text{K}}^0(0) \rightarrow \text{K}_-(\Delta t)]}{P[\text{K}_-(0) \rightarrow \bar{\text{K}}^0(\Delta t)]} \sim \frac{\text{I}(\ell^+, 3\pi^0; \Delta t)}{\text{I}(\pi\pi, \ell^-; \Delta t)}. \quad (6)$$

These quantities can be measured experimentally through numbers of events with certain pairs of decays occurring in time difference Δt . A deviation of these ratios from 1 would be an indication of \mathcal{T} symmetry violation. Bernabeu *et al.* have simulated the behaviour of these ratios expected at KLOE-2 for $10fb^{-1}$ of data ⁴⁾ (Figure 1). At KLOE-2 the asymptotic region of R_2 and R_4 can be observed where their theoretical behaviour may be expressed as:

$$R_2(\Delta t) \xrightarrow{\Delta t \gg \tau_s} 1 - 4\Re\epsilon, \quad (7)$$

$$R_4(\Delta t) \xrightarrow{\Delta t \gg \tau_s} 1 + 4\Re\epsilon, \quad (8)$$

where $\epsilon = (\epsilon_S + \epsilon_L)/2$ is a T-violating parameter ⁴⁾.

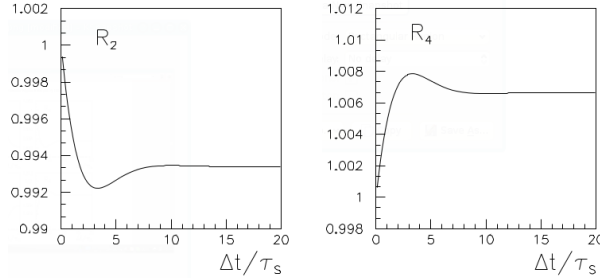


Figure 1: Simulated behavior of the probability ratios expected for $10fb^{-1}$ of KLOE-2 data. The figure was adapted from ⁴⁾.

4 Reconstruction of events for the test

The \mathcal{T} symmetry test requires reconstruction of the processes with $\text{K}_S \rightarrow \pi\pi$, $\text{K}_L \rightarrow \pi^\pm \ell^\mp \nu$ and $\text{K}_S \rightarrow \pi^\pm \ell^\mp \nu$, $\text{K}_L \rightarrow 3\pi^0$ pairs of decays. While for $\text{K}_S \rightarrow \pi\pi$ the $\pi^+\pi^-$ final state can be chosen to take advantage of good vertex and momentum reconstruction from charged pion tracks in the KLOE drift chamber, the $\text{K}_L \rightarrow 3\pi^0 \rightarrow 6\gamma$ decay reconstruction is a challenging task.

This process only involves neutral particles resulting in the calorimeter clusters from six γ hits being the only recorded information. Moreover, this decay has to be reconstructed in cases where the partner K_S decays semileptonically and the missing neutrino prevents the use of kinematic constraints to aid $K_L \rightarrow 3\pi^0$ reconstruction. Therefore, this process requires independent reconstruction.

5 The $K_L \rightarrow 3\pi^0 \rightarrow 6\gamma$ decay vertex reconstruction

The aim of the new reconstruction method is to obtain the spatial coordinates and time of the K_L decay point by only using information on electromagnetic calorimeter clusters created by γ hits from $K_L \rightarrow 3\pi^0 \rightarrow 6\gamma$. Information available for i -th cluster includes its spatial location and recording time (X_i, Y_i, Z_i, T_i) . The problem of localizing the vertex is then in its principle similar to GPS positioning and can be solved in a similar manner.

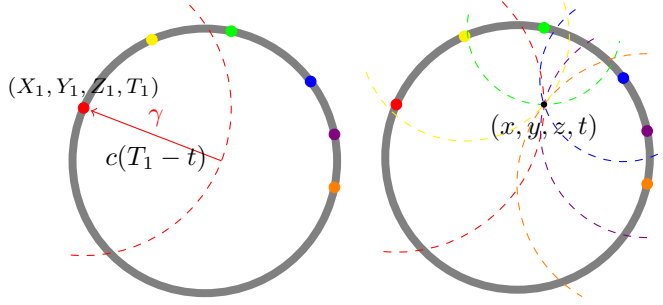


Figure 2: A scheme of $K_L \rightarrow 3\pi^0 \rightarrow 6\gamma$ vertex reconstruction in the section view of KLOE-2 calorimeter barrel (grey circle). Colored dots denote clusters from γ hits. Left: a set of possible origin points of a γ which created a cluster is a sphere centered at the cluster (red dashed line) with radius parametrized by kaon flight time t . Right: intersection point of such spheres for all γ hits is the $K_L \rightarrow 3\pi^0 \rightarrow 6\gamma$ decay point.

For each cluster a set of possible origin points of the incident γ is a sphere centered at the cluster with radius parametrized by an unknown γ origin time t (Figure 2, left). Then, definition of such sets for all available clusters yields a system of up to six equations:

$$(T_i - t)^2 c^2 = (X_i - x)^2 + (Y_i - y)^2 + (Z_i - z)^2 \quad i = 1, \dots, 6, \quad (9)$$

with the unknowns x, y, z and t . It is then easily noticed that the $K_L \rightarrow 3\pi^0 \rightarrow 6\gamma$ vertex is a common origin point of all photons which lies on an intersection of the spheres found as a solution of the above system (Figure 2, right). At least 4 clusters are required to obtain an analytic solution although additional two may be exploited to obtain a more accurate vertex numerically.

It is worth noting that this vertex reconstruction method directly yields kaon decay time in addition to spatial location which is useful for time-dependent interferometric studies such as the \mathcal{T} symmetry test.

Acknowledgments

This work was supported in part by the Foundation for Polish Science through the MPD programme and the project HOMING PLUS BIS/2011-4/3; by the Polish National Science Centre through the Grants No. 0469/B/H03/2009/37, 0309/B/H03/2011/40, 2011/03/N/ST2/02641, 2011/01/D/ST2/00748, 2011/03/N/ST2/02652, 2013/08/M/ST2/00323 and by the EU Integrated Infrastructure Initiative Hadron Physics Project under contract number RII3-CT-2004-506078; by the European Commission under the 7th Framework Programme through the *Research Infrastructures* action of the *Capacities* Programme, Call: FP7-INFRASTRUCTURES-2008-1, Grant Agreement No. 227431.

References

1. L. Wolfenstein, *Int. J. Mod. Phys. E* **8** (1999) 501.
2. A. Angelopoulos *et al.* [CLEAR Collab.], *Phys. Lett. B* **444** (1998) 43.
3. J. Bernabeu, F. Martinez-Vidal and P. Villanueva-Perez, *JHEP* **1208** (2012) 064 [arXiv:1203.0171 [hep-ph]].
4. J. Bernabeu, A. Di Domenico and P. Villanueva-Perez, *Nucl. Phys. B* **868** (2013) 102 [arXiv:1208.0773 [hep-ph]].
5. J. P. Lees *et al.* [BaBar Collab.], *Phys. Rev. Lett.* **109** (2012) 211801
6. J. Beringer *et al.* [Particle Data Group Collab.], *Phys. Rev. D* **86**, 010001 (2012).
7. A. Einstein, B. Podolsky and N. Rosen, *Phys. Rev.* **47** (1935) 777.

Status of measurement of $K_S \rightarrow \pi e \nu$ branching ratio and lepton charge asymmetry with the KLOE detector

Daria Kamińska
on behalf of the KLOE-2 collaboration
Institute of Physics, Jagiellonian University, Cracow, Poland

Abstract

We present the current status of the analysis of about 1.7 billion $K_S K_L$ pair events collected at DAFNE with the KLOE detector to determine the branching ratio of $K_S \rightarrow \pi e \nu$ decay and the lepton charge asymmetry. This sample is ~ 4 times larger in statistics than the one used in a previous KLOE analysis, allowing us to improve the accuracy of the measurement and of the related tests of \mathcal{CPT} symmetry and $\Delta S = \Delta Q$ rule.

1 Introduction

A special role in \mathcal{CPT} violation searches plays a neutral kaon system which, due to a sensitivity to a variety of symmetry violation effects, is one of the best candidates for such kind of studies. One of the possible tests is based on the comparison between semileptonic asymmetry in K_S decays (A_S) and the

analogous asymmetry in K_L decays (A_L)³⁾. So far the A_L ⁴⁾ was determined with a precision more than two orders of magnitude better than A_S ⁵⁾. The present accuracy of A_S determination is dominated by the statistical uncertainty. Therefore the aim of this work is a determination of A_S with two times smaller statistical error due to four times bigger data sample and improved systematical uncertainties. Charge asymmetry is also an important source of information about the real and imaginary parts of the $\mathcal{CP}\mathcal{T}$ violating parameter δ_K . Until now $Re(\delta_K)$ was known with much worse precision than $Im(\delta_K)$.

The measurement was performed using KLOE detector¹⁾ located at DAΦNE accelerator²⁾ in the National Laboratory in Frascati, Italy. The experimental data used in this paper has been collected during data campaign in 2004-2005.

2 Charge asymmetry in neutral kaons semileptonic decays

Neutral kaons are the lightest particles which contain a strange quark. Observed short-living K_S and long-living K_L are linear combinations of strange eigenstates (K^0 and \bar{K}^0):

$$\begin{aligned} |K_S\rangle &= \frac{1}{\sqrt{2(1+|\epsilon_S|^2)}} \left((1+\epsilon_S)|K^0\rangle + (1-\epsilon_S)|\bar{K}^0\rangle \right), \\ |K_L\rangle &= \frac{1}{\sqrt{2(1+|\epsilon_L|^2)}} \left((1+\epsilon_L)|K^0\rangle - (1-\epsilon_L)|\bar{K}^0\rangle \right). \end{aligned} \quad (1)$$

where introduced small parameter ϵ_S and ϵ_L can be rewritten to separate \mathcal{CP} and $\mathcal{CP}\mathcal{T}$ violation parameters ϵ_K and δ_K , respectively:

$$\begin{aligned} \epsilon_S &= \epsilon_K + \delta_K, \\ \epsilon_L &= \epsilon_K - \delta_K. \end{aligned} \quad (2)$$

In the Standard Model decay of K^0 (or \bar{K}^0) state is associated with the transition of the \bar{s} quark into \bar{u} quark (or s into u) and emission of the charged boson. Change of strangeness (ΔS) implies the corresponding change of electric charge (ΔQ) (see Figure 1). This is so called $\Delta S = \Delta Q$ rule. Therefore decays of $K^0 \rightarrow \pi^- e^+ \nu$ and $\bar{K}^0 \rightarrow \pi^+ e^- \bar{\nu}$ are present but $K^0 \rightarrow \pi^+ e^- \bar{\nu}$ and $\bar{K}^0 \rightarrow \pi^- e^+ \nu$ are not. Decay amplitudes for semileptonic decays of states $|K^0\rangle$

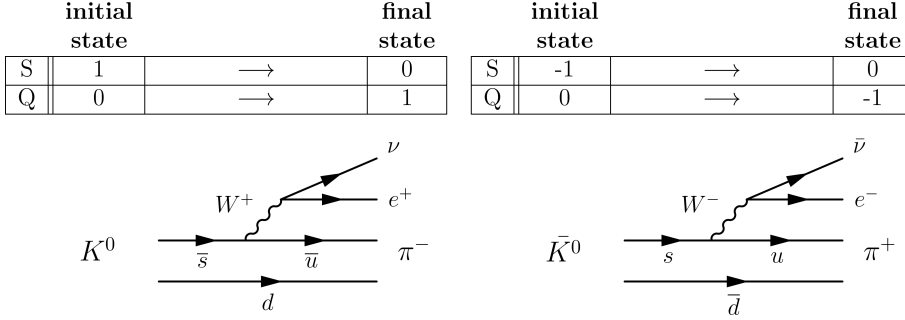


Figure 1: Feynman diagrams for K^0 and \bar{K}^0 semileptonic decay.

and $|\bar{K}^0\rangle$ can be written as follows 3):

$$\begin{aligned}
\langle \pi^- e^+ \nu | H_{weak} | K^0 \rangle &= a + b \\
\langle \pi^+ e^- \bar{\nu} | H_{weak} | \bar{K}^0 \rangle &= a^* - b^* \\
\langle \pi^+ e^- \bar{\nu} | H_{weak} | K^0 \rangle &= c + d \\
\langle \pi^- e^+ \nu | H_{weak} | \bar{K}^0 \rangle &= c^* - d^*
\end{aligned} \tag{3}$$

where the H_{weak} is a part of Hamiltonian corresponding to the weak interaction and a, b, c, d parameters describe the semileptonic decay amplitudes. Applying the symmetry operators to above amplitudes a set of relations between them can be obtained (Table 1). Semileptonic decay amplitudes can be associated with the K_S and K_L semileptonic decay widths through the charge asymmetry ($A_{S,L}$):

$$\begin{aligned}
A_{S,L} &= \frac{\Gamma(K_{S,L} \rightarrow \pi^- e^+ \nu) - \Gamma(K_{S,L} \rightarrow \pi^+ e^- \bar{\nu})}{\Gamma(K_{S,L} \rightarrow \pi^- e^+ \nu) + \Gamma(K_{S,L} \rightarrow \pi^+ e^- \bar{\nu})} \\
&= 2 \left[Re(\epsilon_K) \pm Re(\delta_K) + Re\left(\frac{b}{a}\right) \mp Re\left(\frac{d^*}{a}\right) \right] \\
&\text{if } \Delta Q = \Delta S \\
&= 2 \left[Re(\epsilon_K) \pm Re(\delta_K) + Re\left(\frac{b}{a}\right) \right] \\
&\text{if } \mathcal{CP}\mathcal{T} \text{ and } \Delta Q = \Delta S \\
&= 2 [Re(\epsilon_K)]
\end{aligned} \tag{4}$$

where above equation contains only the first order of symmetry-violating terms. Moreover, conservation of $\Delta Q = \Delta S$ rule and $\mathcal{CP}\mathcal{T}$ symmetry simplifies Equa-

tion 4. Determination the value of charge asymmetry for K_S and K_L allows for tests the fundamental assumptions of Standard Model.

	\mathcal{CP}	\mathcal{T}	\mathcal{CPT}	$\Delta S = \Delta Q$
a	$Im = 0$	$Im = 0$		
b	$Re = 0$	$Im = 0$	$= 0$	
c	$Im = 0$	$Im = 0$		$= 0$
d	$Re = 0$	$Im = 0$	$= 0$	$= 0$

Table 1: Relations between discrete symmetries and semileptonic amplitudes.

The charge asymmetry for K_L decays was precisely determined by KTeV experiment at Fermilab⁴⁾. The measurement was based on 1.9 millions $K_L \rightarrow \pi^\pm e^\mp \nu$ decays produced in collision of proton beam with BeO target. At present the most accurate measurement of K_S charge asymmetry was conducted by KLOE collaboration⁵⁾. Obtained charge asymmetry for K_S decays is consistent in error limits with charge asymmetry for K_L decays which suggest conservation of \mathcal{CPT} symmetry. However, this result is dominated by a statistical uncertainty which is three times larger than the systematic one. Nevertheless it can be improved by analysing 1.7 fb^{-1} total luminosity data sample acquired in 2004 and 2005.

3 Measurement

The KLOE experiment located at DAΦNE ϕ factory is specially suited for analysis of $K_S \rightarrow \pi e \nu$ decay. The KLOE detector is constituted by two main components: a drift chamber and an electromagnetic calorimeter, both inserted into an axial magnetic field (0.52 T). Due to the size of the KLOE drift chamber, about 40% of K_L mesons decay inside the detector while the rest reach the electromagnetic calorimeter. Detection of K_L interaction in the calorimeter allows to identify a K_S meson on the opposite side of ϕ meson decay point.

In order to select semileptonic decay of K_S meson, an additional kinematic selection is applied. It starts from a requirement of a vertex formed by tracks of two oppositely charged particles near the interaction point. Those tracks must be associated to calorimeter clusters. Obtained tracks parameters allow for identification of charged particles in the final state by applying a Time of Flight technique.

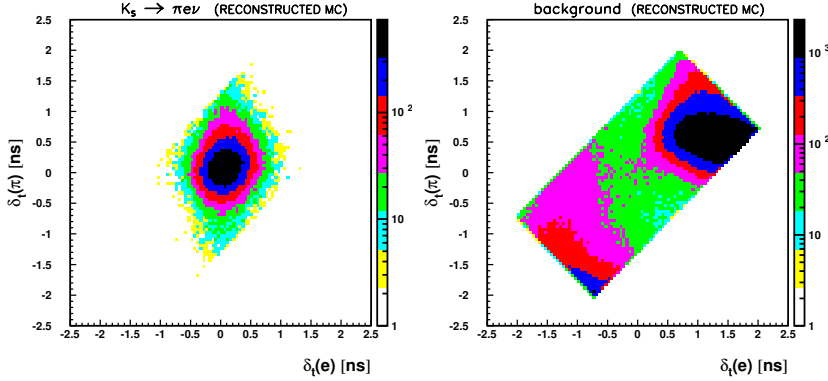


Figure 2: Distributions of the time difference for pion mass hypothesis ($\delta t(\pi)$) versus the time difference for electron mass hypothesis ($\delta t(e)$). Simulations of $K_S \rightarrow \pi e \nu$ and background events are shown on left and right plot, respectively.

For each particle, the difference δ_t between the measured time of associated cluster (t_{cl}) and time of flight is calculated assuming a given mass hypothesis, m_x :

$$\begin{aligned} \delta_t(m_x) &= t_{cl} - \frac{L}{c \cdot \beta(m_x)}, \\ \beta(m_x) &= \frac{P}{\sqrt{P^2 + m_x^2}}, \end{aligned} \quad (5)$$

where L is a total length of particle trajectory and P is particle momentum measured by drift chamber. The Time of Flight technique aims at rejection of the background, which is mainly due to $K_S \rightarrow \pi^+ \pi^-$ events, and at identification of the final charge states ($\pi^- e^+ \nu$ and $\pi^+ e^- \bar{\nu}$). The distribution of difference between missing energy and momentum ($\Delta E(\pi, e)$) shows remaining background components (see Figure 3). Altogether around 10^5 of $K_S \rightarrow \pi e \nu$ decays was reconstructed, which will be used to determine the

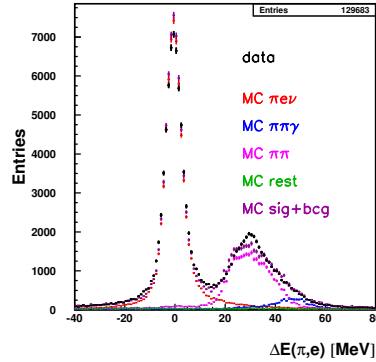


Figure 3: Distribution of $\Delta E(\pi, e) = E_{miss} - p_{miss}$ for all selected events after normalization procedure. Meaning of simulated histograms is described in the legends.

charge asymmetry and branching ratio for K_S semileptonic decays. The analysis is still in progress and preliminary results will be available soon ⁶⁾.

Acknowledgments

This work was supported in part by the Foundation for Polish Science through the project HOMING PLUS BIS/2011-4/3 and the MPD programme; by the Polish National Science Centre through the Grants No. 0469/B/H03/2009/37, 0309/B/H03/2011/40, 2011/03/N/ST2/02641, 2011/01/D/ST2/00748, 2011/03/N/ST2/02652, 2013/08/M/ST2/00323 and by the EU Integrated Infrastructure Initiative Hadron Physics Project under contract number RII3-CT-2004-506078; by the European Commission under the 7th Framework Programme through the 'Research Infrastructures' action of the 'Capacities' Programme, Call: FP7-INFRASTRUCTURES-2008-1, Grant Agreement No. 227431.

References

1. J. Lee-Franzini, P. Franzini, „A Flavor of KLOE”, Acta Phys. Polon. B38 (2007)
2. G. Vignola and DAΦNE Project Team, „DAΦNE, the first ϕ factory”, Conf. Proc. C960610 (1996)
3. L. Maiani, G. Pancheri, N. Paver, „The Second DAΦNE Physics Handbook”, Istituto nazionale di fisica nucleare. Laboratori nazionali di Frascati (1995)
4. KTeV Collaboration, „A measurement of the K_L charge asymmetry”, Phys. Rev. Lett. 88 (2002)
5. KLOE Collaboration, „Study of the branching ratio and charge asymmetry for the decay $K_S \rightarrow \pi e \nu$ with the KLOE detector”, Phys. Lett. B636 (2006)
6. D. Kamińska, „Measurement of the charge asymmetry for the $K_S \rightarrow \pi e \nu$ decay with the KLOE detector”, Master thesis, Jagiellonian University in Cracow (2014)

Frascati Physics Series Vol. LIX (2014), pp. 00-00
4th YOUNG RESEARCHERS WORKSHOP: “Physics Challenges in the LHC Era”
Frascati, May 12 and 15, 2014

**Testing Models with Higher Dimensional Effective Interactions
at the LHC and Dark Matter Experiments**

Martin B. Krauss
INFN, Laboratori Nazionali di Frascati
Via Enrico Fermi 40, 00044 Frascati, Italy

Abstract

New physics can be described by effective field theories in a model independent way. It is possible that the dominant contribution to low-energy effects of new physics is generated by higher-dimensional operators, which are more suppressed than the usually discussed ones. Thus neutrino mass models can be connected to TeV scale physics, for instance. The possible existence of TeV scale particles is interesting, since they can be potentially observed at collider experiments, such as the Large Hadron Collider. Higher dimensional effective operators can also be used to study the interactions relevant for dark matter detection experiments, which we will also discuss.

1 Introduction

Non-zero neutrino masses and the existence of dark matter hint to new physics beyond the Standard Model (BSM). To study BSM physics in a model independent way one can parametrize new physics effects with effective operators \mathcal{O}^d of mass dimension $d > 4$ that are added to the SM Lagrangian:

$$\mathcal{L}_{\text{eff}} = \mathcal{L}_{\text{SM}} + \frac{1}{\Lambda} \mathcal{O}^{d=5} + \frac{1}{\Lambda^2} \mathcal{O}^{d=6} + \frac{1}{\Lambda^3} \mathcal{O}^{d=7} + \dots,$$

where Λ is the scale where the new particles appear. An example is the so called *Weinberg* operator ¹⁾

$$\mathcal{O}_W = LLHH, \tag{1}$$

where L is the SM lepton doublet and H the Higgs boson. After electroweak symmetry breaking it will generate an effective Majorana mass for the neutrinos

$$m_\nu^{\text{eff}} \propto \frac{v^2}{\Lambda}, \tag{2}$$

where $v = \langle H \rangle$ is the VEV of the Higgs boson. Assuming couplings of order one, we can conclude that the scale Λ where the new physics appears is close to the GUT scale, which means it cannot be observed by any current or proposed collider experiments. Recently, however, it has been discussed in literature how neutrino masses can be generated by TeV scale physics. One possibility is that neutrino masses originate from higher-dimensional effective operators, which will be discussed in the following. For more details see ²⁾ and references therein.

2 Neutrino mass from higher-dimensional effective operators

In models that have additional symmetries and further scalar fields (additional Higgs doublets H_u, H_d or scalar singlets S) it is possible that the leading order contribution to neutrino mass is generated by operators with $d > 5$ that are suppressed by higher powers of the new physics scale. ³⁾ ⁴⁾ In this case new particles can appear at the TeV scale, which is of interest for collider experiments such as the LHC. In tab. 1 we show all such operators as extensions of the next-to minimal supersymmetric standard model (NMSSM) up to $d = 9$. Not every of these operators can become the leading contribution to neutrino

	Op.#	Effective interaction	Charge	Same as
$d = 5$	1	LLH_uH_u	$2q_L + 2q_{H_u}$	
$d = 6$	2	LLH_uH_uS	$2q_L + q_{H_u} - q_{H_d}$	
$d = 7$	3	$LLH_uH_uH_dH_u$	$2q_L + 3q_{H_u} + q_{H_d}$	
	4	LLH_uH_uSS	$2q_L - 2q_{H_d}$	
$d = 8$	5	$LLH_uH_uH_dH_uS$	$2q_L + 2q_{H_u}$	#1
	6	LLH_uH_uSSS	$2q_L + 2q_{H_u}$	#1
$d = 9$	7	$LLH_uH_uH_dH_uH_dH_u$	$2q_L + 4q_{H_u} + 2q_{H_d}$	
	8	$LLH_uH_uH_dH_uSS$	$2q_L + q_{H_u} - q_{H_d}$	#2
	9	LLH_uH_uSSSS	$2q_L + q_{H_u} - q_{H_d}$	#2

Table 1: Effective operators generating neutrino mass in the NMSSM up to $d = 9$. Not all of those have a distinct charge from lower-dimensional operators under a discrete symmetry. ⁴⁾

mass, even with an additional discrete symmetry. In the following we want to focus on the $d = 7$ operator $LLH_uH_uH_uH_d$. In the same way the *Weinberg* operator can be decomposed into the type-I, type-II and type-II seesaw ⁵⁾, also this operator has several possible UV-completions. This means that several possible underlying fundamental theories can lead to the same effective operator after integrating out the heavy fields. One example for such a decomposition is shown in fig. 1 and has the superpotential

$$\begin{aligned}
W = & W_{\text{quarks}} + Y_e \hat{e}^c \hat{L} \cdot \hat{H}_d - Y_N \hat{N} \hat{L} \cdot \hat{H}_u + \kappa_1 \hat{N}' \hat{\xi} \cdot \hat{H}_d - \kappa_2 \hat{N}' \hat{\xi}' \cdot \hat{H}_u \\
& + m_N \hat{N} \hat{N}' + m_\xi \hat{\xi}' \cdot \hat{\xi} + \mu \hat{H}_u \cdot \hat{H}_d,
\end{aligned} \tag{3}$$

where N and N' are SM singlets similar to right-handed neutrinos and ξ and ξ' are lepton doublets.

This model has some interesting characteristics. Depending on the mass hierarchy of the mediator fields one can obtain a linear seesaw or an inverse seesaw scenario at an intermediate scale. After integrating out all the fields one obtains in both cases an effective neutrino mass

$$m_\nu^{\text{eff}} \propto \frac{v_u^3 v_d}{\Lambda^3}, \quad \text{with } \Lambda^3 = m_N^2 m_\xi, \tag{4}$$

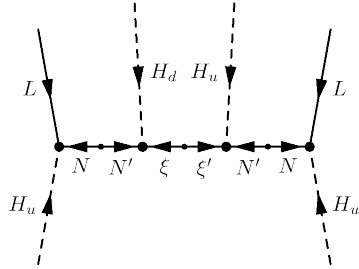


Figure 1: Decomposition of the $d = 7$ operator $(LLH_uH_u)(H_uH_d)$. ⁴⁾

which is at the left-handed neutrino mass scale for $\Lambda \approx \mathcal{O}(1 \text{ TeV})$ for couplings of $\mathcal{O}(10^{-3})$, which is well in the range of the SM Yukawa couplings. This model is also phenomenologically interesting for collider experiments, since it contains doublet fields that can be produced in Drell-Yan processes. Since their mixing to the SM particles is suppressed, they have rather small decay width. As a consequence displaced vertices can appear. One can also study lepton number violating (LNV) processes. Since neutral components of the heavy fermions form so-called pseudo-Dirac pairs one would expect such processes to be very small. This is indeed the case for processes where these heavy states are produced in proton-proton collisions and decay to two same-sign leptons and one W bosons in the final state. In a numerical study, we were able to show that for similar processes with two instead of one W boson we can obtain cross-sections up to 10^{-1} fb , due to the vector like nature of the doublet mediators. ⁴⁾ Another aspect of this model is that the introduction of additional particles can modify the running of the gauge coupling and spoil their unification. This can be avoided by extending the mediators to full multiplets of a GUT gauge group. Due to the limited space we would like to refer the reader to the literature ⁶⁾ for more details.

3 Effective operators and dark matter interactions

Since the nature of dark matter is so far unknown, its interactions with SM particles are usually also described by effective operators.

	(a)	(b)
$d = 5$	—	$\chi\chi H^\dagger H$
$d = 6$	$\chi\chi ff$	$\chi\chi H^\dagger HS$
$d = 7$	$\chi\chi ffS$ $\chi\chi ffH$	$\chi\chi(H^\dagger H)^2$ $\chi\chi H^\dagger HS^2$

Table 2: Higher dimensional operators generating dark matter interactions (a) by direct interactions and (b) via the Higgs portal. ⁷⁾

The leading order operators of DM interactions with SM particles are

$$\mathcal{O}_1 = \frac{1}{\Lambda^2} \chi\chi ff \quad \text{and} \quad \mathcal{O}_H = \frac{1}{\Lambda} \chi\chi H^\dagger H, \quad (5)$$

where χ is the dark matter particle (which we assume to be fermionic for the scope of this discussion) and f is any SM fermion. The second operator \mathcal{O}_H will also lead to interactions of the dark matter particle with SM fermions via the so-called Higgs portal,

$$\mathcal{O}_2 = \frac{1}{\Lambda m_H^2} \chi\chi ff \langle H \rangle. \quad (6)$$

Since, so far, no conclusive evidence of dark matter has been found by direct detection experiments the interaction cross-sections of DM with SM particles has to be small. This is the case when one replaces \mathcal{O}_1 and \mathcal{O}_1 by higher-dimensional operators that are additionally suppressed. In tab. 2 we show a list of such possible operators up to $d = 7$. Other than in the case of the neutrino masses, these leading order operators cannot be avoided by simply introducing a discrete symmetry. Instead one has to study potential models in detail and identify those that generate a higher-dimensional operator without generating the leading order operator at the same time. A systematic study of these operators and their UV-completions ⁷⁾ leads to some interesting observations:

- The UV-completion contains mediators that generate also lower-order operators.
- Scalar mediators with a VEV can induce a lower dimensional operator.

- A mediator is an additional dark matter component that itself has leading order interactions with SM particles.

These complications rule out most of the possible realizations of such a model. There exist, however, options that are not constrained by these considerations. A possible decomposition of the operator $\chi\chi H^\dagger HS$ has the Lagrangian

$$\mathcal{L}_{\#S1} = \mathcal{L}_{\text{SM}} + \lambda_{\chi f\phi} \chi f \cdot \phi + \lambda_{S\phi\phi} S^\dagger \phi \cdot \phi + m_\phi \phi^\dagger \phi + m_\chi \chi\chi + \dots + \text{h.c.} \quad (7)$$

It is testable at the LHC and has interesting phenomenological characteristics.

In summary, effective operators are a powerful tool for studying BSM physics and the additional suppression of higher-dimensional operators has interesting phenomenological consequences that will be tested in current and future collider and dark matter experiments.

Acknowledgments

I would like to thank the organizers of the 4th Young Researcher Workshop at Frascati for giving me the opportunity to present my work. I would like to acknowledge the support by the research training group GRK1147 and the project PO-1337/2-1 of Deutsche Forschungsgemeinschaft (DFG).

References

1. S. Weinberg, *Phys.Rev.Lett.* **43**, 1566 (1979).
2. M. B. Krauss, *Testing Models with Higher-Dimensional Effective Operators at the LHC and Dark Matter Experiments*, PhD thesis, Julius-Maximilians-Universität Würzburg, 2013.
3. F. Bonnet, D. Hernandez, T. Ota, W. Winter, *JHEP* **0910**, 076 (2009).
4. M. B. Krauss, T. Ota, W. Porod, W. Winter, *Phys.Rev.* **D84**, 115023 (2011).
5. E. Ma, *Phys.Rev.Lett.* **81**, 1171 (1998).
6. M. B. Krauss, D. Meloni, W. Porod, W. Winter, *JHEP* **1305**, 121 (2013).
7. M. B. Krauss, S. Morisi, W. Porod, W. Winter, *JHEP* **1402**, 056 (2014).

Frascati Physics Series Vol. LIX (2014), pp. 00-00
4th YOUNG RESEARCHERS WORKSHOP: “Physics Challenges in the LHC Era”
Frascati, May 12 and 15, 2014

Evidence of the SM Higgs boson in the decay channel into τ leptons

Riccardo Manzoni
*Università degli Studi di Milano Bicocca, Italy,
Istituto Nazionale di Fisica Nucleare - sezione di Milano Bicocca, Italy*

Abstract

A search for the standard model Higgs boson decaying into a pair of tau leptons is performed using events recorded by the CMS experiment at the LHC in 2011 and 2012. The dataset corresponds to an integrated luminosity of 4.9 fb^{-1} at a centre-of-mass energy of 7 TeV and 19.7 fb^{-1} at 8 TeV. An excess of events is observed over the expected background contributions, with a local significance larger than 3 standard deviations for m_H values between 110 and 130 GeV.

1 Analysis motivations

After the discovery of a new boson with mass close to 125 GeV, announced by ATLAS ¹⁾ and CMS ²⁾ Collaborations on July 4th 2012, the focus aimed at discerning the properties of this new particle and whether it behaves like the Higgs boson predicted in the Standard Model.

In the SM, the masses of the fermions are generated by the interaction between the Higgs' and the fermions' fields through the Yukawa couplings. The measurements of these couplings are therefore fundamental to completely identify this boson as the SM Higgs boson.

The di- τ decay channel is the most promising, offering low background contamination compared to the $b\bar{b}$ channel and large predicted rate compared to other leptonic channels.

2 Analysis strategy

The analysis ³⁾ is designed to probe the three main Higgs boson production mechanisms at LHC: the gluon fusion, the Vector Boson Fusion (VBF) and the production in association to a W or a Z boson.

2.1 Physics objects

Several physics objects are involved in the analysis: electrons, muons, hadronically decaying taus (τ_h), jets and missing transverse energy (\cancel{E}_T). All of them are built upon the *Particle-Flow* (PF) algorithm ^{4, 5, 6)}, that exploits the information from the all the CMS subdetectors to identify the stable particles generated in the event.

Fig.1 shows the mass of the visible products of the τ_h , reconstructed using the *Hadron Plus Strip* (HPS) algorithm ⁷⁾ that identifies the main decay modes of the τ_h , out of charged hadrons and photons.

2.2 Backgrounds

In the $\mu\tau_h$, $e\tau_h$, $\tau_h\tau_h$ and $e\mu$ channels, the largest source of irreducible background is the Drell-Yan production of $Z \rightarrow \tau\tau$. Other important sources of background are constituted by W+jets processes, contributing significantly to the $\mu\tau_h$ and $e\tau_h$ channels when the W boson decays leptonically and a jet is misidentified as a τ_h , QCD processes, contributing mostly to the $\tau_h\tau_h$ channel when two jets are misidentified as τ_h , and $t\bar{t}$ processes decaying into the fully leptonic, opposite flavor final state, contributing to the $e\mu$ channel.

The Drell-Yan production of $Z \rightarrow \ell\ell$ is the largest background in the $\ell\ell$ channels whilst the di-bosons processes are a relevant source of contamination for the WH and ZH channels.

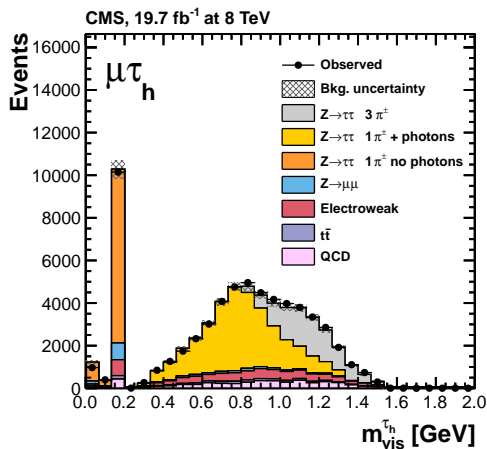


Figure 1: Observed and predicted distributions for the visible τ_h mass, $m_{\text{vis}}^{\tau_h}$, in the $\mu\tau_h$ channel after the baseline selection. The $Z \rightarrow \tau\tau$ contribution is then split according to the decay mode reconstructed by the HPS algorithm as shown in the legend. The mass distribution of the τ built from one charged hadron and photons peaks near the mass of the intermediate $\rho(770)$ resonance; the mass distribution of the τ_h built from three charged hadrons peaks around the mass of the intermediate $a_1(1260)$ resonance. The τ_h built from one charged hadron and no photons are reconstructed with the π^\pm mass, assigned to all charged hadrons by the PF algorithm, and constitute the main contribution to the third bin of this histogram.

All the most important backgrounds are entirely derived from data or controlled in data sidebands.

2.3 Event classification

For the Higgs boson production through gluon fusion and VBF, all the six di- τ final states are considered: $\mu\tau_h$, $e\tau_h$, $\tau_h\tau_h$, $e\mu$, $\mu\mu$, and ee .

The events are then classified in exclusive categories, according to the number of reconstructed jets in the final state and, in particular, the contribution of the VBF production process is enhanced by requiring a large rapidity gap between the two jets with the highest transverse momentum. Moreover, the transverse momentum of the τ (for $\mu\tau_h$, $e\tau_h$ channels) or the μ (for $e\mu$ chan-

nel) and the transverse momentum of the Higgs candidate are used to further split the events in order to enhance the sensitivity.

For the Higgs boson production in association with a vector boson, the presence of one or two additional light leptons, compatible with the presence of a W or a Z boson respectively, is required.

Four channels are considered for at the WH process: $\mu + \mu\tau_h$, $\mu + e\tau_h/e + \mu\tau_h$, $\mu + \tau_h\tau_h$ and $e + \tau_h\tau_h$, whilst eight channels are aimed at ZH process: $\ell\ell + \mu\tau_h$, $\ell\ell + e\tau_h$, $\ell\ell + \tau_h\tau_h$, $\ell\ell + e\mu$, where $\ell\ell$ can be either $\mu\mu$ or ee .

2.4 Signal extraction

The signal extraction is carried out through a global, binned, maximum likelihood fit based on the following final discriminating variables:

- the invariant mass of the di- τ pair, $m_{\tau\tau}$, reconstructed using the SVFIT algorithm ³⁾ from the four momenta of the visible decay products of the Higgs and the \cancel{E}_T , is used for all the channels except for $\mu\mu$, ee and WH;
- the mass of the visible decay products of the Higgs, m_{vis} is used for WH channels. The $m_{\tau\tau}$ is not used because the contributions to the \cancel{E}_T are from both the neutrinos coming from the Higgs and the neutrino coming from the W boson;
- the output distribution of a multivariate discriminator, comprising various kinematic and topological variables, is used for $\mu\mu$ and ee channels

The expected number of signal events is the one predicted by the SM for the production of a Higgs boson of mass m_H decaying into a pair of τ leptons, multiplied by a signal strength modifier μ treated as free parameter in the fit. The contribution from the $H \rightarrow WW$ process, decaying into lepton pairs, ee , $\mu\mu$ or $e\mu$ is non negligible, especially in the $e\mu$ case, and it is treated as background throughout except where explicitly noted.

The systematic uncertainties are represented by nuisance parameters that are varied in the fit according to their probability density function, affecting both the shape and the yields of the different contributions.

3 Results

An excess of events over the background-only hypothesis is observed with a local significance larger than 3 standard deviations for Higgs boson mass hypotheses

between $m_H = 115$ and 130 GeV, and equal to 3.2 standard deviations at $m_H = 125$ GeV, to be compared to an expected significance of 3.7 standard deviations (Fig.2, right). The best-fit value for μ , combining all channels, is $\hat{\mu} = 0.78 \pm 0.27$ at $m_H = 125$ GeV. The mass of the Higgs boson has been measured by performing a scan of the negative log likelihood as a function of mass m_H (Fig.3, left), resulting in a best-fit mass $m_H = 122 \pm 7$ GeV.

The results are compatible with the prediction of a SM Higgs boson at 125 GeV and they constitute the evidence for the coupling between the τ lepton and the Higgs boson discovered by the ATLAS and CMS Collaborations.

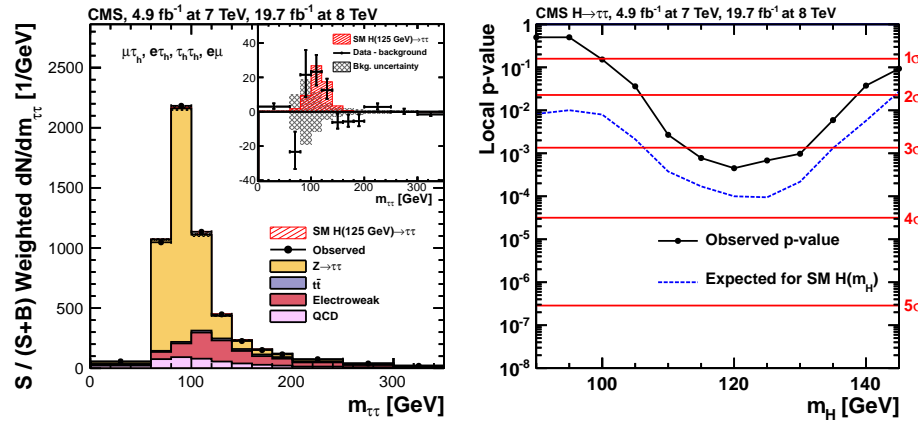


Figure 2: The plot on the left shows the combined observed and predicted $m_{\tau\tau}$ distributions for the $\mu\tau_h$, $e\tau_h$, $\tau_h\tau_h$, and $e\mu$ channels. The signal distribution is normalized to the SM prediction ($\mu = 1$). The distributions obtained in each category of each channel are weighted by the ratio between the expected signal and signal-plus-background yields in the category, obtained in the central $m_{\tau\tau}$ interval containing 68% of the signal events. The inset shows the corresponding difference between the observed data and expected background distributions, together with the signal distribution for a SM Higgs boson at $m_H = 125$ GeV. The plot on the right shows the local p -value and significance in number of standard deviations as a function of the SM Higgs boson mass hypothesis for the combination of all decay channels. The observation (solid line) is compared to the expectation (dashed line) for a SM Higgs boson with mass m_H .

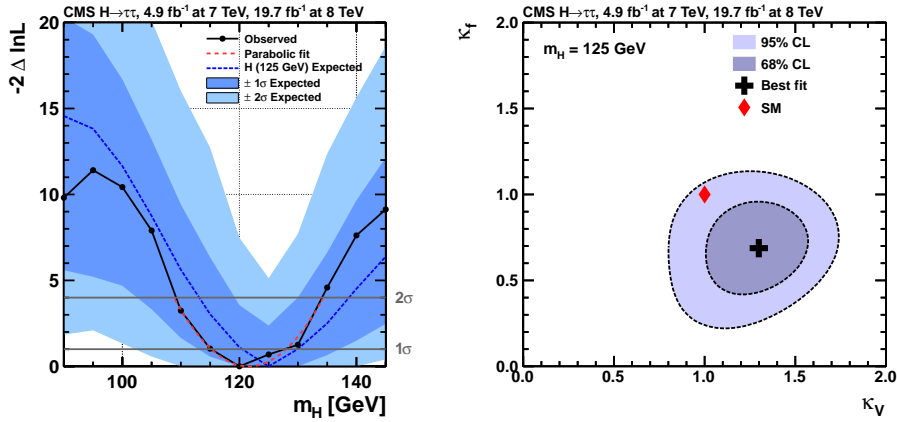


Figure 3: Scan of the negative log-likelihood difference, $-2\Delta \ln \mathcal{L}$, as a function of m_H (left) and as a function of κ_V and κ_f (right). For each point, all nuisance parameters are profiled. The observation (solid line) is compared to the expectation (dashed line) for a SM Higgs boson with mass $m_H = 125$ GeV. For the likelihood scan as a function of κ_V and κ_f , and for this measurement only, the $H \rightarrow WW$ contribution is treated as a signal process.

References

1. ATLAS Collaboration, *Phys. Lett. B* **716**, 1-29 (2012).
2. CMS Collaboration, *Phys. Lett. B* **716**, 30-62 (2012).
3. CMS Collaboration, <http://arxiv.org/abs/arXiv:1401.5041>, (2013).
4. CMS Collaboration, *CMS-PAS-PFT-09-001*, (2009).
5. CMS Collaboration, *CMS-PAS-PFT-10-002*, (2010).
6. CMS Collaboration, *CMS-PAS-PFT-10-003*, (2010).
7. CMS Collaboration, *JINST* **7**, P01001 (2012).

Di-leptons production in top quark decays and New Physics

Néstor Quintero
Physics Department, CINVESTAV-IPN, México City, México,
(*nquintero@fis.cinvestav.mx*)

Abstract

In this work we present the study of the decay $t \rightarrow bW^+\ell^-\ell^+$ ($\ell = e, \mu, \tau$), which diverges for massless di-leptons, and it can reach a branching fraction $\mathcal{O}(10^{-6} - 10^{-5})$ for reasonable values of the low energy cut in the lepton-pair invariant mass. This rate surpasses almost any other rare decays such as $t \rightarrow cX$ ($X = \gamma, Z, g, H, W^+W^-$), and thus offers the possibility of being detectable at the LHC. In addition, we also discuss the same-charge di-leptons production in $\Delta L = 2$ decays $t \rightarrow bW^-\ell^+\ell^+$ as a possible probe of New Physics inducing lepton number violating transitions.

1 Introduction

The top quark is the heaviest fermion in the standard model (SM), and frequently considered as a hint that could help us to understand the nature of electroweak symmetry breaking. Therefore, it is very important a detailed

study of the top quark properties, couplings, production mechanism and decay modes. With a mass of $m_t = 173.34 \pm 0.27 \pm 0.71$ GeV¹ [LHC/Tevatron] ¹), it is known that the top is the only fermion massive enough to undergo first order weak decays, such that its dominant decay channel $t \rightarrow bW^+$. Recently, NNLO QCD corrections to its decay width Γ_t have been calculated ²).

The dominance of the 2-body decay mode $t \rightarrow bW^+$ suppresses considerably any other decay channel, making them hardly detectable. These include the decay modes $t \rightarrow s(d)W^+$, with branching fractions of the order $\text{BR} \sim 10^{-3}(10^{-4})$, which contribute altogether less than one per mille to Γ_t . In the case of 3-body decay modes, the radiative channels $t \rightarrow bW^+\gamma$ ($t \rightarrow bW^+g$) can reach $\text{BR} \sim 10^{-3}(10^{-1})$ for photon (gluon) energy of 5 GeV ^{3, 4}); while for $t \rightarrow bW^+Z$ ^{4, 5, 6, 7}) and $t \rightarrow bW^+H$ ^{4, 7, 8}), the corresponding BR are even smaller. Similarly, the FCNC modes $t \rightarrow cX$ ($X = \gamma, g, Z, H$), $t \rightarrow cW^+W^-(ZZ, \gamma\gamma)$ and $t \rightarrow c\ell^-\ell^+$ ⁹) have an extremely suppressed BR, although some of them involve very interesting dynamical mechanisms and have been suggested as possible probes of New Physics (NP), see for instance ⁹).

In this paper we study the di-lepton production in the 4-body top quark decays $t \rightarrow bW^+\ell^-\ell^+$ ($\ell = e, \mu$ or τ) ¹⁰). The rates of these decays are of order α^2 with respect to $t \rightarrow bW^+$ and have a divergent behavior for massless leptons due to the k^{-2} dependence of the photon propagator. Additionally, we consider the lepton number violating ($\Delta L = 2$) decay $t \rightarrow bW^-\ell_i^+\ell_j^+$, which has been suggested as a signal of New Physics (NP) ^{11, 12}).

2 Four-body decay $t \rightarrow bW^+\ell^-\ell^+$

Let us consider the lepton-pair production in top quark decays $t \rightarrow bW^+\ell^-\ell^+$ with $\ell = e, \mu$ or τ ¹⁰). The relevant diagrams for this decay are shown in Fig. 1. The diagrams Fig. 1(a)-(c) are generated by demanding that the virtual photon (Z boson) converts into a lepton-pair. An additional contribution induced by a neutrino exchange is shown in Fig. 1(d). The full set of diagrams is required in order to fulfill independence upon the electroweak gauge parameters.

The contributions of the Z -boson exchange, as well as the neutrino exchange, are suppressed and the dominant photon-exchange contribution to the amplitude of the channel $t(p_t) \rightarrow b(p_b)W^+(p_W) \ell^-(p_1)\ell^+(p_2)$ is written as ¹⁰

$$\mathcal{M}_{\text{top}}^{\ell^-\ell^+} = \left(\frac{-ige}{\sqrt{2}}\right) V_{tb}^{\text{CKM}} \varepsilon_\mu^W \ell_\nu \bar{u}_b \left[Q_t \mathcal{T}_t^{\mu\nu} + Q_b \mathcal{T}_b^{\mu\nu} + Q_W \mathcal{T}_W^{\mu\nu} \right] u_t, \quad (1)$$

where $\ell_\nu = e[\bar{u}(p_1)\gamma_\nu v(p_2)]/k^2$, with $k = p_1 + p_2$ the virtual photon momentum,

¹In numerical evaluations we use this value of the top quark mass.

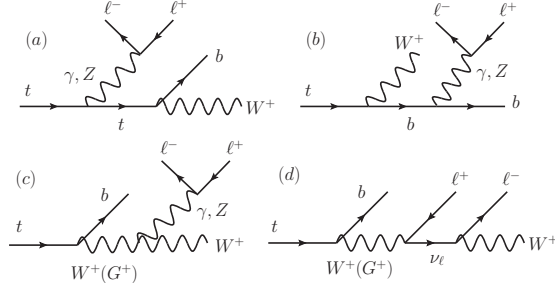


Figure 1: Feynman diagrams that contribute to $t \rightarrow bW^+\ell^-\ell^+$.

(Q_b, Q_t, Q_W) are the particles electric charges in units of e , and ε_μ^W is the four-vector polarization of the W boson. The CKM quark mixing matrix element is taken as $V_{tb}^{\text{CKM}} = 1$. The propagator of the W boson in the unitary gauge is denoted by $\Delta_{\alpha\beta}^W(h) = (-g_{\alpha\beta} + h_\alpha h_\beta / M_W^2) / (h^2 - M_W^2)$, with $h = p_W + k$. The $\mathcal{T}_i^{\mu\nu}(k^2)$ tensors are given by

$$\mathcal{T}_t^{\mu\nu}(k^2) = \gamma^\mu P_L \frac{(p_t - k) + m_t}{k^2 - 2p_t \cdot k} \gamma^\nu, \quad (2)$$

$$\mathcal{T}_b^{\mu\nu}(k^2) = \gamma^\nu \frac{(p_b + k) + m_b}{k^2 + 2p_b \cdot k} \gamma^\mu P_L, \quad (3)$$

$$\mathcal{T}_W^{\mu\nu}(k^2) = \gamma^\alpha P_L \Delta_{\alpha\beta}^W(h) \Gamma_{WW\gamma}^{\beta\mu\nu}, \quad (4)$$

where $\Gamma_{WW\gamma}^{\beta\mu\nu}$ is the triple gauge boson vertex, with our assignment of momenta $W(p_W + k) \rightarrow W(p_W)\gamma(k)$ ¹⁰.

In Figure 2 [Left] we plot the invariant mass distribution of the lepton pair for the three lepton flavors. This observable is peaked close to the threshold for lepton pair production owing to the $1/k^2$ dependence of the photon propagator from the decay amplitude. As it can be checked, this spectrum diverges in the soft limit for massless leptons ($k^2 \rightarrow 0$); making necessary the introduction of an infrared cutoff k_{cut}^2 .

Defining the branching ratio $\text{BR}_{\text{top}}^{\ell^-\ell^+} \equiv \Gamma(t \rightarrow bW^+\ell^-\ell^+) / \Gamma(t \rightarrow bW^+)$, where $\Gamma(t \rightarrow bW^+)$ is the decay width at leading order of the dominant mode of the top quark ¹³, we get values of branching fractions ¹⁰

$$\text{BR}_{\text{top}}^{e^-e^+, \mu^-\mu^+} = 6.31 \times 10^{-6}, \quad \text{BR}_{\text{top}}^{\tau^-\tau^+} = 9.15 \times 10^{-6}, \quad (5)$$

for di-leptons invariant masses larger than $k_{\text{cut}}^2 \geq 20 \text{ GeV}^2$. These results exhibit the good behaviour as determined by the $\mathcal{O}(\alpha^2)$ of the decay rates ¹⁰. In

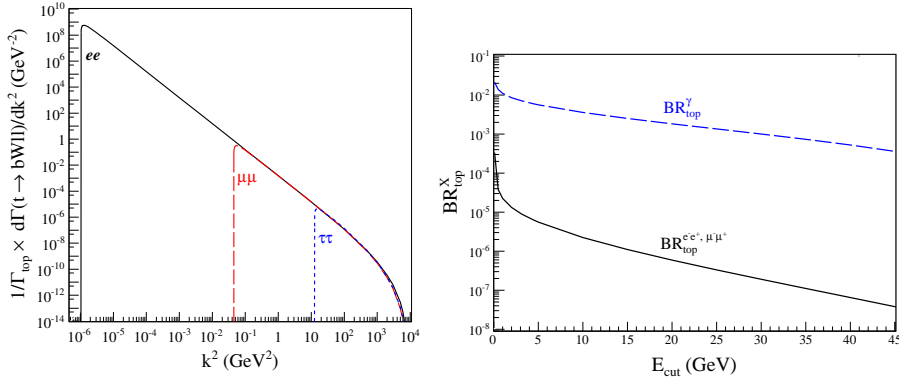


Figure 2: [Left] Normalized invariant-mass distribution for e^-e^+ (solid line), $\mu^-\mu^+$ (long-dashed line) and $\tau^-\tau^+$ (short-dashed line) channels. [Right] Fractions BR_{top}^X as a function of E_{cut} for the radiative channel ($X = \gamma$) and lepton-pair channels ($X = e^-e^+, \mu^-\mu^+$).

addition, for consistency, in Figure 2 [Right] we compare the IR divergent behavior of the decay rates for $t \rightarrow bW^+e^-e^+(\mu^-\mu^+)$ (solid-line) and $t \rightarrow bW^+\gamma$ [see Ref. 10) for details] (dashed-line) as a function of E_{cut} . By notation, in the case of the radiative decay $E_{\text{cut}} = E_{\gamma, \text{cut}}$ corresponds to the photon energy cutoff, while for the four-body channel $E_{\text{cut}} = \sqrt{k_{\text{cut}}^2}$ is the squared root of the invariant mass for the lepton pair. As expected from the perturbative point of view, we observe that these ratios are of order $\mathcal{O}(\alpha^2)$ and $\mathcal{O}(\alpha)$, respectively, for relatively low values of the corresponding IR cutoffs (of the order $E_{\text{cut}} \simeq 3$ GeV).

3 $\Delta L = 2$ decays of the top quark $t \rightarrow bW^-\ell^+\ell^+$

Lepton number violating (LNV) transitions can induce $\Delta L = 2$ processes in 4-body top quark decays to final states containing a same-charge lepton pair (with the same or different flavor): $t \rightarrow bW^-\ell_i^+\ell_j^+$ ($\ell_{i,j} = e, \mu, \tau$). These kind of rare decays are forbidden in the SM and their observation would imply the non-conservation of the lepton number. These $\Delta L = 2$ top quark decays can be mediated by heavy virtual particles that induce LNV transitions as a possible NP effects 11, 12). In particular, a heavy Majorana neutrino with a mass in the range $(M_W + m_{\ell_j}) \leq m_N \leq (m_t - m_b - m_{\ell_i})$ can induce these LNV processes 11), as is shown in Fig. 3.

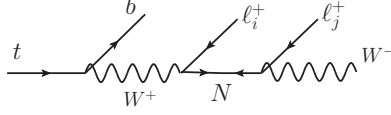


Figure 3: Feynman diagram of $\Delta L = 2$ top quark decays induced by virtual heavy Majorana neutrino (A similar diagram obtained from the lepton exchange $\ell_i \rightleftharpoons \ell_j$ must be added).

The amplitude associated of $\Delta L = 2$ top quark decays is given by ¹¹⁾

$$\begin{aligned}
 (\mathcal{M}_{\text{top}}^{\ell_i^+ \ell_j^+})_N &= i \left(\frac{g}{2\sqrt{2}} \right)^3 V_{tb}^{\text{CKM}} [\bar{u}_b \gamma^\mu (1 - \gamma_5) u_t] \Delta_{\mu\nu}^W(Q) \varepsilon_\alpha^W \\
 &\quad \times V_{\ell_i N} V_{\ell_j N} m_N \bar{u}_i [\mathcal{F}_N \gamma^\nu \gamma^\alpha] (1 - \gamma_5) u_j^c - (\ell_i \rightleftharpoons \ell_j), \quad (6)
 \end{aligned}$$

where $V_{\ell_i N}$ ($V_{\ell_j N}$) is the matrix element of the mixing between charged leptons ℓ_i (ℓ_j) and heavy neutrino N , and $\mathcal{F}_N = [(Q - p_i)^2 - m_N^2 + im_N \Gamma_N]^{-1}$ is the resonant factor, with $(Q - p_i)$, m_N and Γ_N the heavy neutrino virtuality, mass and decay width, respectively. In the case of the same-charge di-lepton channel e^+e^+ , the branching fraction $\text{BR}_{\text{top}}^{\ell_i^+ \ell_j^+} \equiv \Gamma(t \rightarrow bW^- \ell_i^+ \ell_j^+) / \Gamma(t \rightarrow bW^+)$ is very suppressed of the order $\text{BR}_{\text{top}}^{e^+e^+} \lesssim 10^{-13}$, due to the strong constraints that neutrinoless double beta decay impose on the heavy neutrino sector, $\sum_N V_{eN}^2 / m_N < 5 \times 10^{-8} \text{ GeV}^{-1}$ ¹⁴⁾. On the other hand, using the limits on the elements $|V_{\mu N}|^2 < 3 \times 10^{-3}$ and $|V_{\tau N}|^2 < 6 \times 10^{-3}$ that provide electroweak precision test ¹⁴⁾, we get for the channels $\mu^+\mu^+$ and $\tau^+\tau^+$ BR of the order

$$\text{BR}_{\text{top}}^{\mu^+ \mu^+} < 1.4 \times 10^{-7}, \quad \text{BR}_{\text{top}}^{\tau^+ \tau^+} < 6.1 \times 10^{-7}, \quad (7)$$

respectively, for $m_N = 100 \text{ GeV}$.

4 Concluding remarks

In the present work we have studied the di-leptons production in 4-body top quark decays. We have considered the SM allowed channels $t \rightarrow bW^+ \ell^- \ell^+$ as well as the $\Delta L = 2$ channels $t \rightarrow bW^- \ell^+ \ell^+$ that can be induced by a heavy Majorana neutrino. After the restart, it is expected that a centre-of-mass energy of 14 TeV the LHC can reach an integrated luminosity of $\mathcal{L} = 100 \text{ fb}^{-1}$ (or even larger) where it will become in a “top quark factory”. Having about $10^7 - 10^8$ $t\bar{t}$ pairs produced per year, branching fractions of the order $10^{-7} - 10^{-6}$ (as the ones obtained in this work) may be detectable, depending on the signal.

Acknowledgments

The author would like to thank G. López Castro and J. L. Díaz-Cruz for the fruitful collaboration, and Conacyt (México) for financial support.

References

1. ATLAS and CDF and CMS and D0 Collaborations, [[arXiv:1403.4427](#) [[hep-ex](#)]].
2. J. Gao, C. S. Li, and H. X. Zhu, *Phys. Rev. Lett.* **110**, 042001 (2013).
3. G. Tupper, J. Reid, G. Li, and M. Samuel, *Phys. Rev. D* **43**, 274 (1991); G. Couture, *Phys. Rev. D* **40**, 2927 (1989); **42**, 1855(E) (1990); V. Barger, A. Stange, and W.-Y. Keung, *Phys. Rev. D* **42**, 1835 (1990).
4. V. Barger, W.-Y. Keung, and T. G. Rizzo, *Phys. Rev. D* **40**, 2274 (1989); G. Mahlon, [hep-ph/9810485](#); R. Decker, M. Nowakowski, and A. Pilaftsis, *Z. Phys. C* **57**, 339 (1993).
5. G. Altarelli, L. Conti, and V. Lubicz, *Phys. Lett. B* **502**, 125 (2001); J. L. Díaz Cruz and D. A. López Falcon, *Phys. Rev. D* **61**, 051701 (2000).
6. E. Jenkins, *Phys. Rev. D* **56**, 458 (1997).
7. G. Mahlon and S. Parke, *Phys. Lett. B* **347**, 394 (1995).
8. T. G. Rizzo, *Phys. Rev. D* **35**, 1067 (1987); V. D. Barger and W.-Y. Keung, *Phys. Lett. B* **202**, 393 (1988); T. Han and R. Ruiz, *Phys. Rev. D* **89**, 074045 (2014).
9. J. A. Aguilar-Saavedra, *Acta Phys. Polon. B* **35**, 2695 (2004); F. Larios, R. Martínez, and M. A. Pérez, *Int. J. Mod. Phys. A* **21**, 3437 (2006).
10. N. Quintero, J. Lorenzo Díaz-Cruz, and G. López Castro, *Phys. Rev. D* **89**, 093014 (2014).
11. N. Quintero, G. López Castro and D. Delepine, *Phys. Rev. D* **84**, 096011 (2011) [Erratum-*ibid.* *D* **86**, 079905 (2012)]; S. Bar-Shalom, N. Deshpande, G. Eilam, J. Jiang, and A. Soni, *Phys. Lett. B* **643**, 242 (2006); Z. Si and K. Wang, *Phys. Rev. D* **79**, 014034 (2009).
12. N. Quintero, *Phys. Rev. D* **87**, 056005 (2013).
13. J. Beringer *et al.* [Particle Data Group], *Phys. Rev. D* **86**, 010001 (2012).
14. A. Atre, T. Han, S. Pascoli, and B. Zhang, *J. High Energy Phys.* **05**, 030 (2009).

Frascati Physics Series Vol. LIX (2014), pp. 00-00
4th YOUNG RESEARCHERS WORKSHOP: “Physics Challenges in the LHC Era”
Frascati, May 12 and 15, 2014

PERFORMANCE STUDY OF MICROMEGAS MUON CHAMBERS FOR ATLAS UPGRADE

Marco Sessa

on behalf of ATLAS Micromegas Group

Università degli Studi Roma Tre & INFN Sez. di Roma Tre

Via della Vasca Navale 84, 00146 Roma

Abstract

The largest of the ATLAS Phase-1 upgrades of the Muon Spectrometer concerns the replacement of the first muon station of the high-rapidity region with the so called New Small Wheel (NSW), that will be installed during the next Long Shutdown in 2018. The NSW employs Micromegas (MM) and small-strip Thin Gap Chambers (sTGC) detectors, which will allow to reconstruct the muon momentum with a resolution better than 15% at $P_T \sim 1 \text{ TeV}$. In this paper, the performance of MM chambers and, in particular, the spatial resolution and the efficiency, obtained using data from different test beam campaigns, will be described.

1 Introduction

Two long shutdowns, LS2 and LS3, are planned for the ATLAS detector, respectively in 2018 and 2022. After LS3, the luminosity will be increased up to

$6 \div 7 \cdot 10^{34} \text{ cm}^{-2} \text{ s}^{-1}$ and the number of pile-up events will be ~ 200 . Therefore, a very high rate in the forward region of the Muon Spectrometer (especially in the Small Wheel) is expected, with a resulting increase of detectors inefficiency.

The luminosity increase of the LHC will require an upgrade of the ATLAS detector, in order to keep the excellent performance of today in the new running conditions at higher energy. The forward part of the Muon Spectrometer will be replaced with the New Small Wheel (NSW), that will guarantee higher rate capabilities and a better performance for the Level-1 muon trigger. The expected rate at the ultimate luminosity of LHC is expected to be about 15 KHz/cm^2 on the New Small Wheel.

2 Micromegas Technology

Micromegas (MICRO MESH Gaseous Structure) chambers belong to the family of Micro Pattern Gaseous Detectors (MPGD). They consist of a planar electrode (drift cathode), a gas ($\text{Ar} : \text{CO}_2$) gap of 5 mm thickness, acting as conversion and drift region, and a thin metallic mesh positioned at $128 \mu\text{m}$ distance from the readout electrode, creating the amplification region [1]. As shown in Fig.1, charged particles, traversing the drift space, ionize the gas. The electrons, liberated by the ionization processes, drift towards the mesh (in some tens of nanoseconds) and in the thin amplification region the electron avalanche takes place ($\text{Gain} \sim 10^4$). The charge is collected by resistive strips, capacitively coupled to the read-out strips.

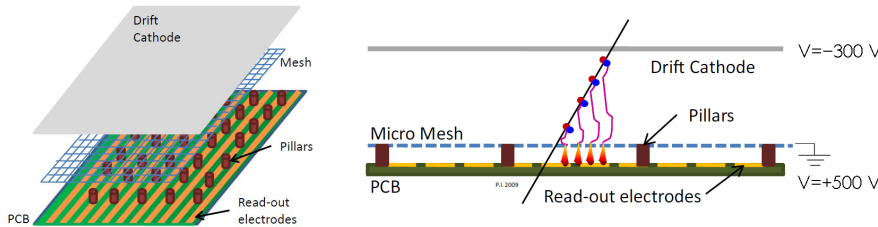


Figure 1: Layout and operating principle of a Micromegas chamber.

3 Track reconstruction

Two methods can be used to reconstruct the point of passage of a particle through the MM chamber.

3.1 Charge Centroid Method

Charge centroid method is based on "neighbouring strips algorithm", that allows to group several fired strips into a cluster. It works very well for tracks perpendicular to the MM chamber [2]. The X coordinate is obtained using the weighted mean shown in (1):

$$X = \frac{\sum_i q_i x_i}{\sum_i q_i} \quad (1)$$

where x_i is the strip position and q_i is the maximum value of the collected charge on that strip. The summation is extended over all strips of a specific cluster.

3.2 μTPC Method

As in the Time Projection Chambers, the μTPC method, used for impact angles larger than 10° , exploits time information in order to obtain the coordinate perpendicular to the readout plane. The drift time (t_{drift}) of the electrons, produced during the ionization processes in the drift region (5 mm thick), is obtained by a Fermi-Dirac fit of time sampled signal of each strip. In this way, using $z-t$ relation ($z = t_{drift} \times v_{drift}$), it's possible also to reconstruct a local track segment in each chamber [3]. Using the gas mixture of $Ar : CO_2$ and the voltages shown in Fig.1, the electrons drift velocity is $\sim 47 \mu m/ns$.

4 Test Beam Data Analysis

The analysis described in this paper has been performed using data recorded during different test beam campaigns, in particular at CERN with $120 \div 150 GeV \pi^-$ and at DESY with an e^- beam of $1 \div 6 GeV$. Two different $10 \times 10 cm^2$ size MM chambers prototypes have been tested:

- Tmm chambers with 250 μm strips pitch and XY readout;
- T chambers with 400 μm strips pitch and X readout.

MM chambers strips are read-out using the APV25 chips, sampling the signal every 25 ns. The test beams, indicated above, offer the possibility to study MM performance under different conditions of angle ($0^\circ \div 40^\circ$), magnetic fields ($0 T \div 1 T$) and operating voltages.

4.1 μTPC optimization

A small angular bias is observed due to capacitive induction of the signal on neighbouring strips. The effect, clearly, is more evident on the first and last strip of the cluster. This causes a small angular bias on the reconstructed tracks, as shown in Fig.2. A possible correction consists in:

- don't use first and last strip if its charge is more than 6 times smaller than its neighbour;
- correct the charge position for the edge strips of the cluster according to:

$$x_{cor}^{first} = \left(\frac{cluster_{length}}{6} \right)^2 \cdot \left(\frac{q_0}{q_1} \right) \cdot \left(\frac{pitch}{2} \right)$$

$$x_{cor}^{last} = \left(\frac{cluster_{length}}{6} \right)^2 \cdot \left(\frac{q_n}{q_{n-1}} \right) \cdot \left(\frac{pitch}{2} \right)$$

After the correction, a significant improvement in the μTPC angular resolution is observed.

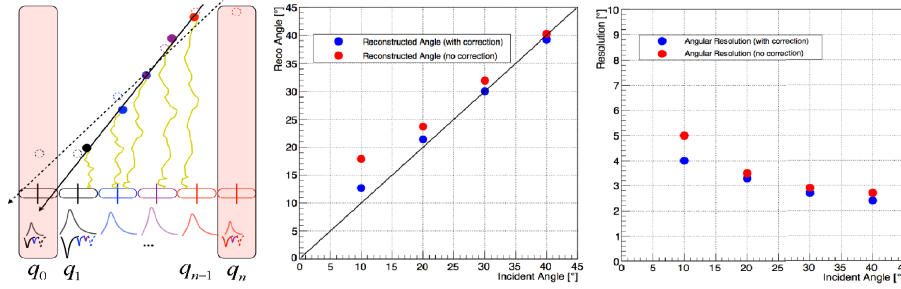


Figure 2: Left: sketch of the capacitive induction of the signals on neighbouring strips. Center: reconstructed angles before and after the correction. Right: angular resolution of a single MM chamber as a function of the beam incidence angle, before and after correction.

4.2 Spatial resolution

The spatial resolution has been studied exploiting both the charge centroid and the μTPC methods. It was measured using two MM chamber (specified by i and j indices) with the same orientation in respect to the beam direction and evaluating the distribution width of the following quantities:

- $\left(x_{centroid}^i - x_{centroid}^j\right) / \sqrt{2}$ for the centroid method,
- $\left(x_{half}^i - x_{half}^j\right) / \sqrt{2}$ for the μTPC method,

in which $x_{centroid}$ is the charge centroid X coordinate while x_{half} is the X coordinate of the track segment, reconstructed using uTPC, at half drift gap.

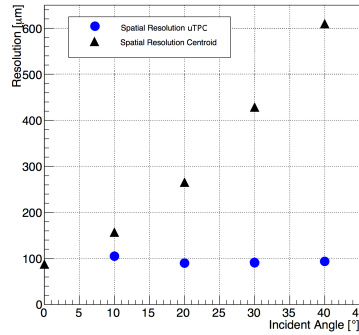


Figure 3: MM spatial resolution as a function of the beam incidence angle (results on July '12 CERN test beam data). In the NSW the typical angles of incidence are expected to be between $8^\circ \div 35^\circ$.

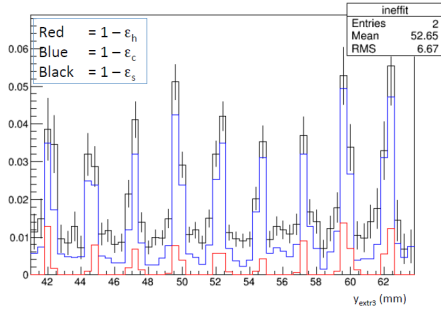
A double gaussian fit was performed in order to take into account the tails of the distribution [4] and the σ of the narrow gaussian has been used as indicator of the resolution, found to be better than $100 \mu m$ in the full angular range, as shown in Fig.3.

4.3 Micromegas inefficiency

The MM chamber inefficiency is obtained by tracking through all chambers but one and looking for missing hits in the test chamber. For this study, June '13 DESY test beam data have been used. The plot in Fig.4 (referred to a T chamber with $HV = 500 V$ and $\theta = 0^\circ$) shows that inefficiencies are mostly

due to the pillars, where the mesh is held tensioned. Pillars have a diameter $300 \mu\text{m}$ and are spaced by 2.5 mm . For this study, three kinds of inefficiencies have been defined:

- **hardware inefficiency** ($1 - \epsilon_h$) \rightarrow no hit in T3 chamber;
- **cluster inefficiency** ($1 - \epsilon_c$) \rightarrow no cluster in T3 chamber;
- **software inefficiency** ($1 - \epsilon_s$) \rightarrow no cluster within 10σ from extrapolated position in T3 chamber.



- $1 - \epsilon_h = 0.19\%$
- $1 - \epsilon_c = 1.34\%$
- $1 - \epsilon_s = 1.95\%$

Figure 4: Inefficiencies as a function of the extrapolated position on T3 chamber.

An average inefficiency less than 2% is observed for runs with tracks at $\theta = 0$, while an efficiency improvement is observed at larger angles.

References

1. The ATLAS Collaboration, New Small Wheel, Technical Design Report, CERN-LHCC-2013-006.
2. M.Iodice *on behalf of the MAMMA Collaboration*, Performance studie of MicroMegas for the ATLAS experiment, IOP Science - Journal of Instrumentation, **9**, 1-15, (2014).
3. C.Bini *on behalf of the MAMMA Collaboration*, Study of the performance of the Micromegas chambers for the ATLAS muon spectrometer upgrade, IOP Science - Journal of Instrumentation, **9**, 1-9, (2014).
4. M. Trovatelli, Performance studies on MicroMegas detector, Il Nuovo Cimento, Vol. 37 C, N. 1, (2014).